

Technical Report, SMU-5-PU

①

AD A095256

LEVEL

PROJECT SQUID

AD A095256

A COOPERATIVE PROGRAM OF FUNDAMENTAL RESEARCH
AS RELATED TO JET PROPULSION
OFFICE OF NAVAL RESEARCH, DEPARTMENT OF THE NAVY

CONTRACT NO0014-79-C-0277

MEASUREMENTS OF THE TRANSVERSE VELOCITY
OF A SEPARATING TURBULENT BOUNDARY LAYER.

1-14

by

Klara Shiloh, B.G./Shivaprasad, and R.L./Simpson

SOUTHERN METHODIST UNIVERSITY

DTIC
ELECTED
FEB 20 1981

June 1980

Published for ONR by
School of Mechanical Engineering
Chaffee Hall
Purdue University
West Lafayette, Indiana 47907

This document has been approved for public release and sale;
its distribution is unlimited.

"Original contains color
plates: All DTIC reproduct-
ions will be in black and
white"

81 2 17 111

DBC FILE COPY

MEASUREMENTS OF THE TRANSVERSE
VELOCITY OF A SEPARATING TURBULENT
BOUNDARY LAYER

by

K. Shiloh*, B. G. Shivaprasad**, and R. L. Simpson***
Southern Methodist University

ABSTRACT

The problem of turbulent boundary layer separation due to an adverse pressure gradient is an old but still important problem in many fluid flow devices. Until recent years little quantitative experimental information was available on the flow structure downstream of separation because of the lack of proper instrumentation. The directionally-sensitive laser anemometer now provides the ability to accurately measure the instantaneous flow direction and magnitude.

Simpson, Chew, and Shivaprasad (1980) presented a number of experimental results for a nominally two-dimensional separating turbulent boundary layer for an airfoil-type flow in which the flow was accelerated and then decelerated until separation. Upstream of separation single and cross-wire hot-wire anemometer measurements were also presented. Measurements obtained in the separated zone with a directionally-sensitive laser anemometer system were presented for U , V , $\overline{u^2}$, $\overline{v^2}$, $-\overline{uv}$, $\overline{u^3}$, $\overline{u^4}$, $\overline{v^3}$, $\overline{v^4}$,

*Visiting Professor of Engineering; permanent address: Israel Atomic Energy Commission, Soreq Nuclear Research Center, Yavne, Israel 70600.

**Visiting Assistant Professor.

***Professor of Mechanical Engineering.

Accession Top	PHO 6-11	By	Director/
	PHO 7-8	Acquisition Codes	
	UNCLASSIFIED		
	DECLASSIFIED		

the fraction of time that the flow moves downstream, the fraction of time that the flow moves away from the wall, and u spectra. In addition to confirming the earlier conclusions of Simpson et al. (1977), these results provided new insights about the separated flow region.

From that work, the backflow appears to be supplied by the large eddy structure rather than coming from far downstream. It also was suggested that downstream of fully-developed separation the mean backflow could be divided into three layers: a viscous layer nearest the wall that is dominated by the turbulent flow unsteadiness but with little Reynolds shearing stress effects; a rather uniform mean velocity intermediate layer that seems to act as an overlap region between the viscous wall and outer regions; and the outer backflow region that is really part of the large-scaled outer region.

For the same flow this report presents experimental results for W , $\overline{w^2}$, $\overline{w^3}$, $\overline{w^4}$, and the fraction of time that the flow moves in one direction across the wind tunnel. A specially-designed directionally-sensitive laser anemometer that is described here was constructed and used to make measurements in the separated region. Cross-wire hot-wire anemometer measurements were obtained upstream of separation and in the outer region of the separated flow and are in good agreement with the laser anemometer results.

The results presented here support the earlier flow model of Simpson et al. (1980). Large scale structures that supply the mean backflow provide a plausible explanation of why u and w related quantities behave as they do in the three near-wall regions mentioned above. These large scale structures transport the turbulence energy to the backflow from the outer flow by turbulent diffusion. This is the main method of providing turbulence energy to

the backflow since advection and production of turbulence kinetic energy is negligible there as compared to the dissipation rate.

NOMENCLATURE

a	$\equiv \tau / \rho q^2$
A_2	$\equiv aF^p$, defined in equation (7)
a_1, a_2, b_2, c_1, c_2	functions of time in equations (2)
C_1	defined in equation (8)
C_2	$\equiv C_1 F^{1/4}$, defined in equation (9)
$C_f/2$	$\equiv \tau_w / \rho U_\infty^2$, local skin-friction coefficient
F	ratio of total turbulence energy production to shear production, equation (6)
F_u, F_v, F_w	$\overline{u^4}/(\overline{u^2})^2$, $\overline{v^4}/(\overline{v^2})^2$, and $\overline{w^4}/(\overline{w^2})^2$ kurtosis or flatness factor for u, v, and w fluctuations, respectively.
H_{12}	$\equiv \delta_1/\delta_2$, velocity profile shape factor
P	mean pressure
p	exponent in equation (7)
$\overline{q^2}$	$\overline{u^2} + \overline{v^2} + \overline{w^2}$
Re_{δ_2}	$\equiv U_\infty \delta_2 / \nu$, momentum thickness Reynolds number
S_u, S_v, S_w	$\overline{u^3}/(\overline{u^2})^{3/2}$, $\overline{v^3}/(\overline{v^2})^{3/2}$, and $\overline{w^3}/(\overline{w^2})^{3/2}$ skewness factors for u, v, and w fluctuations, respectively
U, V, W	instantaneous velocity components in x, y, z directions, respectively
U, V, W	mean velocities in x, y, z directions, respectively
u, v, w	instantaneous fluctuations velocities in x, y, z directions, respectively

u', v', w'	rms fluctuation velocities in x, y, z directions, respectively
$-\overline{uv}, -\overline{uw}$	Reynolds shearing stresses
U_τ	$\equiv (\tau_w/\rho)^{1/2}$, shear velocity
U^+	$\equiv U/U_\tau$
x, y, z	streamwise, normal, and spanwise coordinates
y^+	$\equiv yU_\tau/\nu$
$Y_{1/2}$	perpendicular distance from reference streamwise line to where U is $U_\infty/2$ for mixing layer of Wignanski and Fiedler.

Greek Symbols

$\gamma_{pu}, \gamma_{pv}, \gamma_{pw}$	fraction of time the flow moves downstream, away from the wall, and in the transverse direction, respectively
δ	y where $U = 0.99 U_\infty$
δ_1	$\equiv \int_0^\infty (1 - U/U_\infty) dy$, displacement thickness
δ_2	$\equiv \int_0^\infty (U/U_\infty)(1 - U/U_\infty) dy$, momentum thickness
ϵ	rate of turbulent energy dissipation in equation (4)
ν	kinematic viscosity
ρ	density
τ	shearing stress

Subscripts

w	denotes wall value
∞	denotes free-stream condition

ACKNOWLEDGMENTS

The authors would like to thank Mr. Bob Turner, who made special optical mounts, and Mr. Francis Isely, laboratory manager, who was helpful in many ways. Dr. R.E. Nasburg and J. Sallas kept the data acquisition computer operational. Judy Whirley and Arlene Armbruster put the figures, tables, and manuscript into the present form.

TABLE OF CONTENTS

	Page
ABSTRACT	i
NOMENCLATURE	iv
ACKNOWLEDGMENTS	vi
TABLE OF CONTENTS	vii
I. INTRODUCTION	1
II. EXPERIMENTAL EQUIPMENT	4
A. Hot-wire Anemometer Probe	4
B. Laser Anemometer	7
1. Basic features of the optical system	8
2. Details of the optical system	10
3. Signal processing	11
4. Particle seeding	13
5. Measurement uncertainties	13
6. Alignment procedure	15
III. EXPERIMENTAL RESULTS	15
A. Mean Velocity Results	16
B. Turbulence Results	17
C. Skewness and Flatness Factor Results	19
IV. DISCUSSION OF RESULTS	20
A. Reynolds Normal Stresses	20
B. Turbulence Energy Dissipation Rate Near the Wall	23
C. Reynolds Stresses Correlations	25
V. CONCLUSIONS - The Nature of the w Component in a Separating Turbulent Boundary Layer	27

	Page
VI. FUTURE WORK	30
REFERENCES	31
APPENDIX-Tabulated Laser and Hot-wire Anemometer Data	33

I. INTRODUCTION

The problem of turbulent boundary layer separation due to an adverse pressure gradient is an important factor in the design of many devices such as jet engines, rocket nozzles, airfoils and helicopter blades, and the design of fluidic logic systems. Until the last six years little quantitative experimental information was available on the flow structure downstream of separation because of the lack of proper instrumentation.

In 1974 after several years of development, a one-velocity-component directionally-sensitive laser anemometer system was used to reveal some new features of a separating turbulent boundary layer (Simpson et al., 1974). The directional sensitivity of the laser anemometer system was necessary since the magnitude and direction of the flow must be known when the flow moves in different directions at different instants in time. In addition to much turbulence structure information, it was determined: (1) that the law-of-the-wall velocity profile is apparently valid up to the beginning of intermittent separation; (2) that the location of the beginning of intermittent separation or the upstreammost location where separation occurs intermittently is located close to where the freestream pressure gradient begins to rapidly decrease; (3) that the normal stress terms of the momentum and turbulent kinetic energy equations are important near separation; and (4) that the separated flowfield shows some profile similarity of the streamwise velocity U , of the velocity fluctuation u' , and of the fraction of time that the flow moves downstream (Simpson et al., 1977).

Based upon these results, modifications (Simpson and Collins, 1978; Collins and Simpson, 1978) to the Bradshaw et al. (1967) boundary layer prediction method were made with significant improvements. However, this

prediction effort pointed to the need to understand the relationship between the pressure gradient relaxation and the intermittent separation region structure. A number of other workers have tried to predict this type flow, but with questionable assumptions about the turbulence structure near the wall. In nearly all efforts, the workers have simply extended the velocity and turbulence profile correlations that apply to attached flows to the backflow region. Even though turbulent fluctuations near the wall in the backflow region are as large as or larger than mean velocities, these predictors used a turbulence model that is tied to the mean velocity gradient. Even with adjustment of turbulence model "constants" to fit one feature or another, these models do not predict simultaneously the backflow velocity profile, the streamwise pressure distribution, and the fact that length scales increase along the flow. Clearly then, a limiting factor for further improvement of the prediction of separated flows is the lack of fundamental experimental velocity and turbulence structure information with which to develop adequate models, especially for the backflow region.

Simpson, Chew, and Shivaprasad (1980) presented experimental results for a nominally two-dimensional separating turbulent boundary layer for an airfoil-type flow in which the flow was accelerated and then decelerated until separation. Upstream of separation single and cross-wire hot-wire anemometer measurement results were presented. Measurements were obtained in the separated zone with a directionally-sensitive laser anemometer system for U , V , $\overline{u^2}$, $\overline{v^2}$, $-\overline{uv}$, $\overline{u^3}$, $\overline{v^3}$, $\overline{u^4}$, $\overline{v^4}$, the fraction of time that the flow moves downstream γ_{pu} , fraction of time that the flow moves away from the wall γ_{pv} , and u spectra.

In addition to confirming the earlier conclusions of Simpson et al.

(1977) regarding a separating airfoil-type turbulent boundary layer, these results provided new insights about the separated region: (1) The backflow mean velocity profile scales on the maximum negative mean velocity U_N and its distance from the wall N . A U^+ vs. y^+ law-of-the-wall velocity profile is not consistent with this result. (2) The turbulent velocities are comparable with the mean velocity in the backflow, although low turbulent shearing stresses are present. (3) Mixing length and eddy viscosity models are physically meaningless in the backflow. (4) Negligible turbulence energy production occurs in the backflow.

These and other results led Simpson et al. (1980) to significant conclusions about the nature of the separated flow when the thickness of the backflow region is small as compared with the shear layer thickness. The backflow is controlled by the large-scale outer region flow. The small mean backflow does not come from far downstream, but appears to be supplied intermittently by large-scale structures as they pass through the separated flow. Downstream of fully-developed separation, the mean backflow appears to be divided into three layers: a viscous layer nearest the wall that is dominated by the turbulent flow unsteadiness but with little Reynolds shearing stress effects; a rather flat intermediate layer that seems to act as an overlap region between the viscous wall and outer regions; and the outer backflow region that is really part of the large-scaled outer region flow. The Reynolds shearing stress must be modeled by relating it to the turbulence structure and not to local mean velocity gradients. The mean velocities in the backflow are the results of time-averaging the large turbulent fluctuations and are not related to the source of the turbulence.

For the same flow this report presents experimental results from along

the tunnel centerline for W , $\overline{w^2}$, $\overline{w^3}$, $\overline{w^4}$, and the fraction of time that the flow moves in one direction across the wind tunnel. A specially-designed directionally-sensitive laser anemometer was constructed and used to make measurements in the separated region. Cross-wire hot-wire anemometer measurements were obtained upstream of separation and in the outer region of the separated flow. The next section describes this experimental equipment. Section III describes the experimental results and section IV discusses the meaning of these results. Section V presents the implications of these results on our understanding of the nature of W in a separating turbulent boundary layer.

II. EXPERIMENTAL EQUIPMENT

Simpson et al. (1980) used and described in some detail the same wind tunnel, boundary layer control system, and test flow as used in the current series of experiments. The description of these aspects will not be repeated here since the results presented here supplement the earlier results. In other words, both reports are required anyway to obtain all of the measurement results on the test flow.

The same hot-wire anemometers and electronics, used by Simpson et al. (1980) were used in this research. However, the probe and the alignment technique required for satisfactory W measurements are significantly different to warrant further discussion. An entirely new laser anemometer optical arrangement was required to measure W , as described below.

II.A. Hot-Wire Anemometer Probe

The hot-wire probe was a standard TSI Model 1248-TT.5 end-flow minia-

ture cross-wire probe. Each wire is inclined at 45° to its sensor supports. In use one wire is sensitive to $u + w$ fluctuations while the other is sensitive to $u - w$. The probe stem or the 0.06 inches O.D. stainless steel tube containing the sensor supports was mounted perpendicular to the probe holder and permitted measurements as close as 0.05 inches from the surface. The two platinum-plated tungsten wire sensors, 0.00015 inches diameter and 0.05 inches long, are only 0.02 inches apart, which produces less effect of large streamwise velocity gradients on the measurements than wider spacings.

A TSI Model 1127 Calibrator was used for calibrating the probe. There was no detectable drift of the anemometers. The linearizers had a small amount of D.C. drift. This was nulled with a small D.C. offset corresponding to the no flow condition before starting the calibration for each experiment. Each linearized calibration had a small deviation from a straight-line, with a product moment correlation coefficient (Bragg, 1974) in excess of 0.9999. The slopes of each calibration were repeatable within $\pm 4\%$ over the entire series of experiments.

A TSI Model 1015C Correlator was used to instantaneously add and subtract the linearized $u + w$ and $u - w$ signals obtained from the two wires. Two Analog Devices AD533JH four-quadrant multipliers were used, one in the squaring mode and the other in the multiplying mode to obtain u^2 , w^2 , $(u + w)^2$, w^3 , and w^4 . The nonlinearity error for the multipliers were approximately $\pm 2\%$ of the full scale output voltage of 10 (volts)². The time-averaging was done using true-integrating voltmeters consisting of a voltage-controlled oscillator (Tektronics FG501 and Wavetek Model 131) and a digital frequency counter (Tektronics DC 503 Universal Counter and Anadex CF - 600). Measurements with the true-integrating voltmeters were repeat-

able within $\pm 1\%$. The overall frequency response of the hot-wire anemometer and its associated instrumentation was flat up to 7.5 kHz.

To properly align the sensors with respect to the probe holder, the plane formed by the probe stem and the probe holder was mounted perpendicular to the calibrator flow. The probe stem was rotated within the hole in the probe holder until the voltages obtained from both wires were a minimum. Thus, both wires were inclined at 45° to the calibration flow direction. The setscrew was tightened to lock the probe stem to the probe holder in that position. This process insured that each wire was in the xz plane when the probe holder was aligned with the y direction.

To ensure that the probe stem axis and hence the planes containing the two wires are parallel to the x-axis in the test flow, the probe was mounted in the wind tunnel such that the sensors were close to the bottom test wall. Since the bottom wall was a highly polished wooden surface the reflected image of the probe stem was visible to the naked eye. The probe holder fixed to the traversing mechanism was rotated about the z-axis such that the stem and its image were visibly parallel. Finally, to ensure that both the wires were inclined to the x direction at 45° , the probe was moved to the freestream and the probe holder was rotated about the y-axis until the velocities obtained from the individual signals and the sum of the two signals were within 1% of one another.

In summary, the uncertainties for the hot-wire measurements due to all of these sources are: U , $\pm 3\%$; $\overline{u^2}$, $\pm 8.2\%$; $\overline{w^2}$, $\pm 12.5\%$; S_w , ± 0.1 ; F_w , ± 1.0 ; $-\overline{uw}$, $\pm 1(\text{fps})^2$. Measurements in the separated region were confined to regions where the instantaneous flow direction made an angle less than 45° with the mean flow direction.

A motorized traversing mechanism as described by Strickland and Simpson (1973) was used for traversing the x-wire probe across the boundary layer. It had a probe positioning uncertainty of ± 0.001 inches. In addition, a cathetometer was used to locate the probe sensor near the wall within an uncertainty of approximately ± 0.002 inches.

II.B. Laser Anemometer

The basic requirements of a w component laser anemometer are that it be directionally-sensitive, that it have high y -direction spatial resolution, and that it have high enough signal-to-noise ratio and signal data rate to produce well-defined velocity probability histograms. Ideally one would like to add the w component measuring system to the existing U and v measuring system described by Simpson and Chew (1979) and Simpson et al. (1980) and use the same optical window in the wind tunnel as used for U and v measurements.

This is only possible using a reference beam approach where the incident laser beam is parallel to the w direction. Orloff and Logan (1973) and Kreid and Grams (1976) have developed such confocal backscattering reference beam anemometers. However, they require an etalon to increase the coherence length of the laser and a good optical table for precise alignment of the received signal and the reference beam. Due to delivery time limitations, both of these requirements could not be met in time for this research. However, this approach using a self-aligning decoupling beamsplitter-combiner design (Kreid and Grams, 1976) appears promising and is currently being developed by others (Adrian, 1979; Kiland, 1979).

A second approach is a dual beam system where the incident laser beams enter through the wind tunnel bottom and form real fringes that are

perpendicular to the W direction. This approach has all of the advantages of a fringe system over a reference beam system; it permits a large received signal aperture, produces higher signal-to-noise ratio (SNR) signals for sparse seeding, does not require critical beam alignment to obtain good signals, does not require an etalon as long as incident beam paths are equal, and does not require a high quality optical table. Figure 1 is a schematic of this approach, which was used to obtain the results presented here.

The length of the signal-producing focal volume was too long to obtain the required y -direction spatial resolution using forward or back scattering. Thus, the signal was collected at right angles to the incident beams as shown in Figure 3. The photomultiplier tube aperture was opened enough to obtain signals from only a small portion of the focal volume height.

II.B.1. Basic features of the optical system

Several drawbacks of this optical system should be noted.

- (a) The laser beams have a long and cumbersome path to the bottom of the tunnel.
- (b) Glass windows had to be flush-mounted into the bottom wall of the wind tunnel.
- (c) Alignment of the plane of the beams with the W component is difficult due to the short distance between the beams compared to the tunnel width. This alignment is critical since U is much larger than W and poor alignment causes the laser anemometer to measure $U \sin \xi + W \cos \xi$, where ξ is the misalignment angle. Alignment is also important since the angle of the mean flow with respect to the tunnel axis is an important measure of mean flow three-dimensionality.

(d) Only a small portion of the focal volume length can be used, leaving the sampling volume and signal data rate to be controlled by the focal volume diameter rather than the focal volume length as in forward or backscattering arrangements. The focal volume diameter can be increased, as done here, but this reduces the laser power concentration and hence the SNR. Previous experience (Simpson et al., 1980) with a backscattering arrangement showed that neither the signal data rate nor the signal-to-noise ratio were abundant. However, the greater intensity of right angle scattering appears to partially overcome the disadvantage of the small signal producing volume. The smoke concentration was doubled over that previously used to also improve the data rate.

There are also several positive features of this optical arrangement:

- (a) The signal is easily distinguished from the light scattered by the window at the beams entrance except very close to the wall.
- (b) The SNR tends to be improved over forward or backscattering because less light from the main laser beams outside the focal volume is collected with the signal. In this arrangement these laser beams are separated by the focal volume length rather than the focal volume diameter as in forward or backscattering arrangements.
- (c) The long beam paths enables the small splitting angle of the Bragg cell to develop a sufficient beam spread that no additional mirrors are required. Thus the velocity to signal frequency relationship is constant since the beam spacing at lens L_3 remains constant.
- (d) The path lengths of the incident beams are equal for minimum laser noise effects.

II.B.2. Details of the optical system

Since the measuring volume in this optical arrangement is governed by the focal volume diameter, primary consideration in the optical system design was given to obtain a focal volume diameter that produced good SNR signals at a sufficiently high rate. Too large a focal volume diameter produces low SNR signals due to laser power limitations. On the other hand too small a focal volume diameter produces too low a signal data rate due to a small number of particles in the focal volume. An intermediate diameter was selected that produced both a high SNR and a good signal data rate. Table 1 lists the important values for the resulting optics. As shown in Figures 1 and 2, lenses L_1 and L_2 and the final focusing lens L_3 were used to determine the beam diameter and to produce parallel ray beams that crossed at the focal volume. This produced parallel fringes without requiring that the two beams cross at their waists as in the case of converging-ray beams. The Bragg cell split the initial laser beam into two equal power beams with one frequency shifted 24.55 MHz. This produced fringes that moved through the focal volume at the Bragg-shifted frequency and made the laser anemometer directionally-sensitive. In other words, W motions in one direction produced signals greater than the Bragg frequency while W motions in the other direction produced signals less than the Bragg frequency.

Aside from the mirrors that manipulate the laser beams, the only other important component in the incident beams system is the optical flat. As shown in Figures 1 and 3, rotation of the optical flat permits sensitive streamwise adjustment of one of the incident laser beams so that the plane of the laser beams can be aligned with the W velocity component.

The signal-receiving lens L_4 , photomultiplier tube, and interference

Table 1. Characteristic Dimensions of the W
Component Optical System

Component	Parameter	Value
Lens L_1	Focal length	-14.9 mm
Lens L_2	Focal length	48 mm
	Distance between L_1 and L_2	25 mm
	Beam diameter at L_2	5 mm
Lens L_3	Focal length	0.432 m
	Distance from laser to L_3	2.44 m
	Beam diameter at L_3	0.9 mm
	Angle between incident beams	2.84 degrees
	Fringe spacing	9.8 μm
	Crossing volume length	30.5 mm
	Crossing volume diameter	0.75 mm
Lens L_4	Focal length	0.416 m

filter are the same as used by Simpson et al. (1980). A slit or an iris diaphragm was used as the aperture. Near the wall where $\partial U/\partial y$ is large, the dioctyl phthalate smoke particle concentration is sufficiently high that a horizontal slit of height 0.01 inches provides a good signal data rate and good spatial resolution. Farther away from the wall the smoke concentration is lower and $\partial U/\partial y$ is lower so that the iris with up to 0.08 inches opening can be used.

II.B.3. Signal processing

Signal processing was by fast-sweep-rate sampling spectrum analysis, with the same equipment as described by Simpson and Barr (1975) and Simpson and Chew (1979). The signal processing logic is as follows. The signal from the photomultiplier tube or detector is put into a swept filter spectrum analyzer. For each sweep of the filter when a signal is detected, a vertical voltage distribution proportional to the filter output is displayed. The simultaneous horizontal sweeping voltage is proportional to the signal frequency. The peak of the vertical voltage distribution marks the frequency of the passing particle signal and can be used as a gating signal to allow the instantaneous value of the horizontal sweep voltage E to be sampled. This instantaneous voltage value is related to the instantaneous velocity w of the particle through

$$w = \lambda_f (f_0 - f_B + \left(\frac{df}{dE}\right)E) = \lambda_f (f - f_B) \quad (1)$$

where λ_f is the fringe spacing, f_0 is the analyzed frequency at the beginning of a sweep, f_B is the Bragg cell frequency, and df/dE is a calibration constant relating the analyzed frequency to the horizontal sweep voltage.

Prior to gating the horizontal sweep voltage, the vertical voltage distribution is fed into a peak detector circuit which produces a pulse simultaneously with the occurrence of the first peak value. In the circuit used here a 1 μ sec wide pulse is produced. This output pulse is used to trigger a sample-and-hold circuit, into which the horizontal sweep voltage has been fed. The sampled sweep voltage E is held by the sample-and-hold circuit until a new signal from another particle is detected. This output voltage E is fed to a probability analyzer where a velocity probability histogram was obtained. W , $\overline{w^2}$, $\overline{w^3}$, $\overline{w^4}$, and the fraction of time that the W flow is positive γ_{pw} can be obtained from each histogram. As pointed out by Simpson and Chew (1979) and Simpson et al. (1980), the equal-time-interval sampling by the probability analyzer of the sample-and-hold output voltage results in a true time-averaged histogram shape rather than an average over the number of signals obtained.

The vertical voltage signal peak must be distinguishable above the wideband noise level for detection. The discrimination level must be above the highest noise level present in the range of Doppler frequencies for the turbulence present. Since the signal is processed in the frequency domain, the signal-to-wideband-noise ratio need not be as good as signals processed in the time domain with counters. A resolution bandwidth of 1% to 3% of the frequency analyzer dispersion and a sweep rate between 200 and 1000 Hz was used. The sweep rate was set equal to the sampling rate of the probability analyzer, which was about twice the average data signal rate of the sample-and-hold circuit. For most of these experiments, the discrimination level was set at 8dB, permitting a data signal rate of 100-200 Hz.

Considerable effort was spent to verify that the resulting histograms

were nearly independent of the discriminator level. Data were obtained with the discrimination level set at 3dB, which produced an apparent data signal rate close to 1000 Hz, but resulted in a wideband noise contribution to the histogram. Selecting the proper noise level for a given histogram required some subjective judgment. However, when this noise was subtracted from a histogram, the resulting histogram was closely the same as the corresponding one without noise that was obtained at an 8dB discrimination level. Clearly, the data obtained with a high discriminator level are preferred.

II.B.4. Particle seeding conditions

The 1 micron dioctyl phthalate particles follow the highly turbulent oscillations found in separated regions (Simpson and Chew, 1979). It is, of course, impossible to seed a highly turbulent flow in any prescribed manner. This is not really important since equal-time-interval sampling by the probability analyzer produces a histogram that is independent of the particle concentration. Based on the estimates given by Echols and Young (1963) there are about 131,000 particles per cubic inch.

At this concentration the number of particles in the volume at any time varies between 0.13 when using the slit aperture to 0.9 for the iris aperture. These conditions correspond to the loss of signal or drop-out 87% to 10% of the time, respectively. These results are consistent with the observation that at a 1000 Hz sweep rate the data rate is only 200 Hz to 300 Hz, i.e., signals only occur 20% to 30% of the time.

II.B.5 Measurement uncertainties

The major source of uncertainty in these measurements is the drift of the spectrum analyzer. The drift fluctuated at a very low frequency, corresponding to about ± 1.5 fps for a five-minutes buildup of a histogram.

Near the wall and near the freestream it took only one minute to construct a histogram and the drift was proportionally less.

The influence of this drift on the results calculated from histograms was examined using actual histograms and assuming a flat distribution for the drift. In other words, for each velocity in a histogram it was assumed to have an equal probability to be within ± 1.5 fps of that value. Computations showed that the mean velocity was uncertain within ± 1.5 fps for the bulk of the measurements. This value decreased to about ± 0.3 fps near the wall and near the freestream. Because the fraction of the velocity histogram that is positive, γ_{pw} , depends on where the zero velocity is located, these larger uncertainties make γ_{pw} highly uncertain.

The drift had little practical effect on the variance $\overline{w^2}$. For high variances greater than $5 \text{ ft}^2/\text{sec}^2$, it contributed about $1 \text{ ft}^2/\text{sec}^2$. For low variances the experiment time was short and the drift was smaller. In this latter case the drift contributed about $0.8 \text{ ft}^2/\text{sec}^2$ to the variance.

The skewness and flatness are decreased by the drift. Values for near gaussian histograms are affected no more than 20% for the skewness and 5% for the flatness. For significantly non-gaussian distributions that occur near the wall and near the freestream, the effect is about the same because the time to construct these histograms was less and the drift was less. In essence the effect of the drift is to make the histogram more gaussian.

Other factors produced minor uncertainties. The uncertainty in the angle between the two laser beams and the uncertainty in the spectrum analyzer frequency-to-voltage calibration produce an uncertainty of $\pm 2\%$ in the instantaneous velocity. Velocity gradients across the focal volume produce a broadening in the histogram of about $0.25 \text{ ft}^2/\text{sec}^2$.

In summary, taking into account all of these sources of uncertainty, the maximum uncertainties for the laser anemometer results reported here are: W , ± 1.5 fps; $\sqrt{w^2}$, ± 1.0 fps using a 3dB discriminator level, ± 0.5 fps using a 8dB discriminator level; S_w , ± 0.2 ; F_w , ± 1.0 . The distance of the measurement volume from the test wall is about ± 0.002 inches uncertain while the movement of the traversing apparatus is about ± 0.001 inches uncertain. These uncertainty estimates are consistent with the observed scatter in the results presented in section III below.

II.B.6. Alignment procedure

As mentioned in section II.B.1 alignment of the plane of the laser beams with the y component is critical in order to avoid contaminating the measurements with u . First the laser beams are focused in the freestream. Then the optical flat shown in Figure 3 and described in section II.B.2 above is rotated until the resulting w is repeatably zero well within the uncertainty of ± 1.5 fps. The remaining data within the profile are obtained with the optical flat in the same position while traversing toward the test wall.

III. EXPERIMENTAL RESULTS

While this report is mainly devoted to measurements related to w , for the sake of continuity several features of this flow that were measured by Simpson et al. (1980) are presented here. Figure 5 shows the freestream velocity distribution along the wind tunnel centerline while Figure 6 shows the mean flow pattern in the vicinity of separation. (One should not let the mean flow streamlines leave the impression that the backflow is supplied from far downstream. Large scale structures appear to supply the backflow

locally.)

The flow has a favorable pressure gradient that becomes adverse downstream of 58 inches. Pressure gradient relaxation starts near 105 inches and remains at a minimum value downstream of 156 inches. Intermittent backflow is first observed 1% of the time at 122 inches, which is denoted by ID in Figure 6. Downstream the fraction of time that the backflow occurs increases until a mean backflow is observed near 136 inches. The backflow increases in extent downstream until at 173 inches it occupies one-third of the boundary layer thickness.

Representative measurements of w related quantities were obtained in the several regions of this flow. Hot-wire anemometer measurements were obtained near the beginning of the adverse pressure gradient region near 64 inches. Laser and hot-wire anemometer measurements were obtained at 115 inches just upstream of the beginning of intermittent separation and at 126 inches in the intermittent separation region. Measurements near 138 inches were obtained for a low mean backflow while those at 160 and 173 inches are for the well-developed backflow region. These results are tabulated in the Appendix.

III.A. Mean Velocity Results

Mean velocities in the longitudinal direction U were measured as a by-product during the measurement of w turbulence quantities with the cross-wire probe. Figures 7 show nondimensional velocity profiles of these results and the corresponding velocity profiles obtained by Simpson et al. (1980). The boundary layer thickness values obtained from the present data were used to nondimensionalize both sets of data. Both sets of data agree with-

in their uncertainties.

The angle between the free-stream flow direction and the tunnel centerline was measured by the hot wire and laser anemometers and is given in Table 2 for the several streamwise measurement locations. Since the free-stream flow is moving slightly across the tunnel toward the optics, there is a non-zero component of mean velocity perpendicular to the tunnel centerline. Table 2 also shows the free-stream W results when the plane of the optics was aligned perpendicular to the tunnel centerline. These values are only greater than the W measurement uncertainty at the last two streamwise locations.

<u>x location</u>	<u>Angle towards optics</u>	<u>W, fps, with reference to tunnel centerline</u>
115.50	0.6° ± 0.2°	0.6 ± 1.5 fps
138.67	1.3° ± 0.2°	1.1 ± 1.5 fps
160.33	2.6° ± 0.2°	2.0 ± 1.5 fps
173.25	2.9° ± 0.2°	2.2 ± 1.5 fps

Table 2. Angle between free-stream flow direction and tunnel centerline and free-stream crossflow velocity, laser anemometer data.

Within the boundary layer flow W varied randomly about zero within the measurement uncertainties up to the 138 inches location. Downstream W/U_∞ increased with distance to 0.04 at 173 inches, with an uncertainty of ± 0.03.

III.B. Turbulence Results

The turbulent intensities in the longitudinal direction u'/U_∞ were also obtained as a by-product during the hot-wire measurements. Figures 8 give a comparison of the profiles of u'/U_∞ between the present data and those of Simpson et al. for various streamwise stations. By referring to the above mentioned uncertainties, one can observe that the discrepancy between the two sets of data lies within the uncertainties at all stations except the downstream most one at 173-1/4 inches. Nevertheless, this general agreement between the two sets of data instills confidence in these hot-wire measurements.

Figure 9 gives the lateral turbulent intensity profiles at all the stations using both the laser and the hot-wire anemometers. In general, the two sets of data agree with one another within their total uncertainty limits at most locations. However, at 173-1/4 inches the agreement is not satisfactory. Still, the good agreement observed in Figure 9 for most of the stations with the established hot-wire technique gives confidence in the dual beam technique of measurement of w' with the laser anemometer.

Figure 10 gives the distributions of the turbulent kinetic energy across the boundary layer at the various stations. At most of the stations it was not possible to use the hot-wire probe for making measurements of u' all across the boundary layer, and hence both u' and v' values were taken from the data of Simpson et al. (1980) which were obtained for the same flow conditions as the present one. Since the location of some of the stations for the present measurements were slightly different from those for their data, the values of u' and v' at the same x and y locations were obtained by curve fitting and interpolation. A five-point quadratic curve-fitting program was used to obtain the U , u' , and v' and $-\overline{uv}$ values at the same y locations corresponding to the present data while linear interpolation

was used to obtain values at the required x locations. $\overline{q^2}$ is about $\pm 6\%$ uncertain.

Figure 11 shows the non-dimensional distributions of the Reynolds shear stress, $-\overline{uw}/U_\infty^2$. This was measured using the hot-wire probe only and hence the data are restricted to the region near the outer edge of the boundary layer. Upstream of separation and at the last two downstream locations, $-\overline{uw}/U_\infty^2$ lies within the measurement uncertainty of 5×10^{-4} . At 125 and 138 inches there is a definite trend of $-\overline{uw}$ being definitely negative nearer the wall. The ratio $-\overline{uw}/-\overline{uv}$ is of the order -0.4 in the middle part of the boundary layer at these two locations, but with an uncertainty of ± 0.3 . Upstream and downstream of these locations $-\overline{uw}/-\overline{uv}$ is about -0.1 , also with an uncertainty of ± 0.3 . These results indicate a non-zero $-\overline{uw}$ near the beginning of separation that would lead to mean flow three-dimensionality downstream. This is consistent with the previously mentioned observations that the mean flow is slightly three-dimensional downstream of separation.

III.C. Skewness and Flatness Factor Results

Figures 12 and 13 give the distributions of the flatness F_w and skewness S_w factors upstream of separation. Both figures show agreement between the laser and hot-wire anemometer results within the uncertainties. Near the wall F_w rises substantially above the gaussian value of 3, as was the case for F_u and F_v reported by Simpson et al. (1980). S_w is nearly independent of distance from the wall and is slightly positive, although it is within the experimental uncertainty of being zero for a two-dimensional mean flow.

Figures 14 and 15 show the laser anemometer results downstream of separation. These figures also show the results of Wagnanski and Fiedler (1970) for the low velocity side of a plane mixing layer. As in the case of the u and v fluctuations (Simpson et al., 1980) these two types of flow have similar distributions for S_w and F_w . Also as in the case of the u and v fluctuations, S_w and F_w tend to achieve profile similarity from just upstream of separation. This means that separation does not have any special effect on S_w and F_w . Since F_w is close to 3 and S_w is close to zero, the w fluctuations are nearly gaussian over the middle portion of the boundary layer and separated shear layer.

To the authors' knowledge no other data for S_w and F_w are available for attached boundary layers upstream of separation and for separated shear layers.

IV. DISCUSSION OF RESULTS

IV.A. Reynolds Normal Stresses

Figures 16 give a comparison of the distributions of u'^2/U_∞^2 , v'^2/U_∞^2 and w'^2/U_∞^2 at the several streamwise locations. One can notice that v'^2 and w'^2 are approximately equal in the outer 90% of the boundary layer at most of the locations. Near the wall, w'^2 is greater than v'^2 at all locations. This feature is consistent with the measurements of Sandborn and Slogar (1955) in an adverse pressure gradient boundary layer approaching separation.

The data of Schubauer and Klebanoff (1950) for a boundary layer approaching separation at 25.4 ft. also indicate similar trends. However, their data for w'^2/U_∞^2 at the beginning of adverse pressure

gradient region are much higher than v'^2/U_∞^2 over almost the entire boundary layer. This is different from the trends observed in the present data at 63 13/16 inches and those at station 1 of Sandborn and Slogar in the corresponding region of measurement. As shown in Table 3, the momentum thickness Reynolds numbers at these locations in the present and Sandborn and Slogar studies are 2900 and 2700, respectively, whereas the Schubauer and Klebanoff flow has a value of 18750. Bradshaw's (1967) adverse pressure gradient equilibrium turbulent boundary layer flow also has w'^2 larger than v'^2 at Re_{δ_2} of 22900. This leads one to infer that in addition to the differences in the way the pressure gradient varies before becoming adverse, the Reynolds number may have an effect in distributing the turbulent kinetic energy between the three modes of fluctuations. As the flow approaches separation however, the Reynolds number does not seem to have much effect and w'^2 approaches v'^2 in the outer region.

Table 3: Some flow conditions for the present and previous investigations

Parameter	Streamwise location (in inches) for the present data		Data of other investigators				
			Streamwise location (in ft.) for Schubauer and Klebanoff's data			Station no. for Sandborn and Slogar's data	
	63.813	115.5	17.5	24.5	25.4	1	4
Re_{δ_2}	2900.6	11000	18750	57792	70011	2700	7930
H_{12}	1.357	1.86	1.35	1.99	2.39	1.362	1.673
$\frac{1}{2}C_f \times 10^3$	1.724	0.538	1.73	0.25	0.04	1.75	0.825
$\beta = \frac{\delta_1}{\tau_w} \frac{dP_\infty}{dx}$	0.1	11.9	0	28.8	187.1	0.09	4.3

Figures 17 show that w'/u' and v'/u' are not only nearly equal within the uncertainty of ± 0.1 but remain nearly constant in the range of 0.55 to 0.65 for $0.1 < y/\delta < 0.7$. The magnitude of the w'/u' maximum near the wall generally increases with downstream distance. Near the outer edge the uncertainties associated with the small values of u' , v' , and w' lead to the wide deviation shown. Figure 18 shows that w'/u' for the present data compares well with the data of Sandborn and Slogar and Schubauer and Klebanoff just upstream of separation for the conditions given in Table 3.

Another important result shown in Figures 16 is the inflexional shapes of the u'^2/U_∞^2 and w'^2/U_∞^2 distributions near the wall. From 115-1/2 inches and downstream, the slope of u'^2/U_∞^2 first increases with y/δ and then decreases at inflexion point A to a constant value over a short region before increasing again at inflexion point B. Also from 115-1/2 inches and downstream, w'^2/U_∞^2 increases for a short distance and then remains constant from inflexion point C until it is almost equal to v'^2/U_∞^2 at inflexion point D. As shown in Figures 17, point C coincides with the local near wall maximum in w'/u' . Point D occurs at a y/δ of 0.1 for the four streamwise locations for which data are available.

Points C and D also have special significance in regard to profiles of \bar{v} related data. Figure 7(b) shows that downstream of fully-developed separation, point C corresponds closely to the position of minimum mean velocity U . Point D occurs at a slightly higher velocity. Figures 19 and 20 show that point C closely corresponds to the minima in the upstream-downstream intermittency γ_{pu} and the intermittency of the flow away from the wall γ_{pv} . Figure 21, which is Figure 43(b) of Simpson et al. (1980), shows that points C and D lie on opposite sides of the hump in the

flatness factor F_u . The hump itself shows that relatively large u fluctuations occur infrequently in this region, indicating the intermittent passage of very high and very low velocity fluid with respect to the mean velocity.

Figure 22 shows no special significance for points C and D, except that they lie in the region of increasing correlation of Reynolds shear-stress-producing u' and v' motions. Point A seems to be near where \overline{uv} is first significantly greater than zero.

Figure 23 shows the turbulence energy balance at 156 3/8 inches. No significant turbulence energy production occurs closer to the wall than point D. The next section relates the near wall data to the turbulence energy dissipation rate.

IV.B. Turbulence Energy Dissipation Rate Near the Wall

Some insight about the turbulence energy balance near the wall can be gained by relating the measured near wall structure to the turbulence energy dissipation rate. From the continuity equation and the no-slip condition at the wall, the equations for the velocity fluctuations nearest the wall

$$u = a_1 y + a_2 y^2 \dots \quad (2a)$$

$$v = b_2 y^2 + \dots \quad (2b)$$

$$w = c_1 y + c_2 y^2 \dots \quad (2c)$$

can be written, where a_1 , a_2 , b_2 , c_1 , and c_2 are functions of time. After squaring each side of each equation and time averaging the result one obtains

$$\overline{u^2} = \overline{a_1^2} y^2 + 2\overline{a_1 a_2} y^3 + \overline{a_2^2} y^4 + \dots \quad (3a)$$

$$\overline{v^2} = \overline{b_2^2} y^4 + \dots \quad (3b)$$

$$\overline{w^2} = \overline{c_1^2} y^2 + 2\overline{c_1 c_2} y^3 + \overline{c_2^2} y^4 + \dots \quad (3c)$$

At the wall and very close to the wall, the mean turbulence energy dissipation rate can be expressed as (Rotta, 1962)

$$\frac{\epsilon}{\nu} = \overline{\left(\frac{\partial u}{\partial y}\right)^2} + \overline{\left(\frac{\partial w}{\partial y}\right)^2} \quad (4)$$

Using equations (2) in equation (4) produces

$$\frac{\epsilon}{\nu} = (\overline{a_1^2} + \overline{c_1^2}) + 4(\overline{a_1 a_2} + \overline{c_1 c_2})y + \dots \quad (5)$$

$\overline{a_1^2}$ and $\overline{c_1^2}$ can be estimated well using equations (3) and the measured $\overline{u^2}$ and $\overline{w^2}$ data, while $\overline{a_1 a_2}$ and $\overline{c_1 c_2}$ are much more uncertain to obtain.

Table 4 presents the results at the wall for the four locations at which $\overline{w^2}$ data are available. While $\epsilon\delta/U_\infty^3$ is approximately constant within the $\pm 20\%$ experimental uncertainty, ϵ/ν at the wall decreases by an order of magnitude over the region of separation.

Location, inches	$\epsilon\delta/U_\infty^3 \times 10^3$	$(\epsilon/\nu) \times 10^{-6} \text{Sec}^2$
115 1/2	4.2	23
138 2/3	3.6	4.6
160 1/3	3.7	2.3
173 1/4	4.2	2.3

Table 4. Estimated turbulence energy dissipation rate at the wall

Figure 23 shows all of the non-dimensional turbulence energy balance terms for a separated flow location except the dissipation rate and the diffusion near the wall. $\epsilon\delta/U_\infty^3$ is much larger nearest the wall than the

advection and turbulence energy production terms, so the turbulence energy diffusion rate near the wall must be equally large for an energy balance. This result confirms the suggestion by Simpson et al. (1980) that turbulence energy is transported to the backflow region by diffusion where it is dissipated.

IV.C. Reynolds Stresses Correlations

Several turbulence correlations involving w'^2 were examined by Simpson et al. (1980) for this separating turbulent boundary layer. However at that time they made the assumption that $w'^2 = 1/2 (u'^2 + v'^2)$, which East and Sawyer (1979) had made, in order to evaluate $\overline{q^2}$. Now that the present w'^2 data show that this assumption is not valid for separating boundary layers, the turbulence correlations given by Simpson et al. that involve w'^2 must be revised.

Figure 24 gives the distributions of $-\overline{uv}/\overline{q^2}$ across the boundary layer for the several streamwise stations at which w'^2 data are available. The peaks in the $\overline{q^2}$ profiles shown in Figures 10 closely coincide with the peaks in the $-\overline{uv}$ profiles shown in Figures 16e and 16f of Simpson et al. (1980) since $-\overline{uv}/\overline{q^2}$ remains flat in the middle part of the boundary layer with an uncertainty of ± 0.01 . The distribution given by Bradshaw (1967) for a zero pressure gradient boundary layer is also plotted as a solid line in the figure. One can notice good agreement between Bradshaw's distribution and the present data at the 63.81 inches station which is far upstream of the regions of strong adverse pressure gradients and separation.

As noted by Simpson et al. (1980), $-\overline{uv}/\overline{q^2}$ in the vicinity of separation and downstream is smaller than upstream and has no universal distribution near the wall. As done by Simpson et al. (1977), Simpson et al. (1980)

accounted for this reduction in $-\overline{uv}/q^2$ by the fact that normal stresses turbulence energy production as well as shear stress turbulence energy production are responsible for the magnitude of q^2 . It is the purpose of this section to account for this reduction in the value of $-\overline{uv}/q^2$ from 0.15 to 0.09 in the same manner as discussed in Simpson et al. (1980), but using measured values of w'^2 . Results for the three streamwise locations with available w'^2 data are given in Table 5.

The ratio of total turbulence energy production to shear stress production is

$$F = 1 - \frac{(u'^2 - v'^2) \partial U / \partial x}{-\overline{wv} \partial u / \partial y} \quad (6)$$

Using this factor evaluated at the maximum shearing stress location, the correlation for $-\overline{uv}/q^2$ could be modified as

$$(-\overline{uv}/q^2)F^p = A_2 = 0.15 \quad (7)$$

Table 5 indicates an average value of about 1.25 for p instead of 1.33 obtained by Simpson et al. (1980).

Collins and Simpson (1978) related u'^2 and v'^2 to q^2 at the maximum shearing stress location by

$$(u'^2 - v'^2) = C_1 q^2 \quad (8)$$

The present flow data fit the following expression better

$$(u'^2 - v'^2) = C_2 q^2 / F^{1/4} \quad (9)$$

Table 5 indicates an average value of 0.43 for C_2 , instead of 0.37 obtained by Simpson et al. (1980).

Table 5: Parameters computed to account for the effect of normal stresses on some turbulence correlations.

x in inches	y/δ at max $-\overline{uv}$ location	F from eqn(6)	$\frac{-\overline{uv}}{q^2}$	C_2	P	A_2	$\frac{C_2}{A_2}$	F from eqn(10)
115.5	0.246	1.22	0.117	0.4	1.23	0.151	2.65	1.26
138.67	0.455	1.69	0.090	0.49	0.98	0.173	2.86	1.56
160.33	0.633	1.45	0.089	0.4	1.41	0.141	2.86	1.56

The deviation of this average value from the individual C_2 values is within the experimental uncertainty of $\pm 26\%$ involved in its evaluation.

Using eqns. (6), (7), and (9) with a p of 1.25 one obtains

$$F = \frac{1}{1 + \frac{C_2}{A_2} \frac{\partial U / \partial x}{\partial U / \partial y}} \quad (10)$$

Using tabulated values for A_2 and C_2 obtained from eqns. (7) and (9), respectively, the ratio C_2/A_2 was computed and given in Table 5. An average value is 2.79 with an uncertainty of 0.17 instead of 2.5 as reported by Simpson et al. (1980). As shown in Table 5, F values calculated from eqn. (10) using this average value agree within the experimental uncertainty of $\pm 14\%$ with F values derived directly from eqn. (6).

V. CONCLUSIONS - The Nature of w in a Separating Turbulent Boundary Layer.

The results presented here for w related quantities supplement the measurements of U and V related quantities by Simpson et al. (1980). The physical interpretation of these results is consistent with that presented in that report. It was suggested that downstream of fully-developed separation the mean backflow could be divided into three layers: a viscous layer nearest the wall that is dominated by the turbulent flow unsteadiness but with little Reynolds shearing stress effects; a rather flat intermediate layer that seems to act as an overlap region between the viscous wall and outer regions; and the outer backflow region that is really part of the large-scaled outer region flow.

For reference the most important results from the present data are summarized below.

1. $w'^2 = v'^2$ in the outer 90% of the shear layer upstream and downstream of separation.
2. Inflexion points in the u'^2 and w'^2 distributions seem to have some significance. The u'^2 inflexion point nearest the wall in the backflow is near the zero $-\overline{uv}$ location and the outer edge of the viscous layer. The w'^2 inflexion point nearest the wall in the backflow appears to coincide with the positions of minimum mean velocity U , minimum upstream-downstream intermittency γ_{pu} , and minimum γ_{pv} intermittency of the flow away from the wall. F_w is greater than 3 between the wall and this inflexion point and is about 3 farther from the wall. Between this w'^2 inflexion point and the next one, which bracket the overlap region, w'^2 is about constant and F_u has a local maximum. No significant turbu-

lence energy production occurs closer to the wall than this second w'^2 inflexion point.

3. The turbulence energy dissipation rate at the wall, as deduced by u'^2 and w'^2 data near the wall, is much larger than the advection and turbulence energy production rate in the backflow, so turbulence energy diffusion must be equally large to balance the dissipation rate.
4. The basic correlation relationship between $-\overline{uv}$ and u'^2 , v'^2 , and w'^2 remain the same as estimated by Simpson et al. (1980), although the empirical constants are slightly different. The correlation constants presented here should be used since actual w'^2 data were used rather than an estimate.
5. While the mean test flow is not perfectly two-dimensional, the basic nature of a mean two-dimensional separating flow is illustrated since the streamwise flow is the main source of momentum and kinetic energy. The mean crossflow W is only a little larger than the measurement uncertainty. S_w , the skewness for w , is about zero within the measurement uncertainty, as it should be for a mean two-dimensional flow.

Clearly, the behavior of W related quantities is closely connected to the behavior of U and V related quantities. As mentioned by Simpson et al. (1980) the backflow is supplied locally by outer region large-scale structures, at least for cases where the thickness of the mean backflow region is small compared to the shear layer thickness. As a large structure of the order of δ in height and width supplies fluid toward the wall in the

separated region, v fluctuations decrease and are exactly zero on the wall. Because of continuity requirements the fluid must be deflected and contribute to u and w fluctuations. Thus u' and w' are a little greater due to this wall effect than they would be with large scale structure effects alone. This explains why u' and w' distributions have the inflexion points near the wall. No plausible explanation of these data appears possible when the mean backflow is required to come from far downstream.

VI. FUTURE WORK

Currently a scanning laser anemometer system is being developed to obtain almost instantaneous velocity profiles. These data should prove useful in relating the instantaneous backflow to the outer region flow.

REFERENCES

1. Adrian, R. T. 1979 Private Communication.
2. Bradshaw, P. 1967 "The Turbulence Structure of Equilibrium Boundary Layers", J. Fluid Mech., 29, pp. 625-645.
3. Bradshaw, P. 1973 "Effects of Streamline Curvature on Turbulent Flow", AGARDograph No. 169.
4. Bragg, G. M. 1974 Principles of Experimentation and Measurement, Prentice-Hall, Englewood Cliffs, N.J.
5. Collins, M. A. and Simpson, R. L. 1978 "Flowfield Prediction for Separating Turbulent Shear Layers", AIAA J., 16, pp. 291-292.
6. Cole, J. B. and Swords, N. D. 1979 "Laser Doppler Anemometry Measurements in an Engine", Appl. Optics, 18, No. 19, pp. 1539-1545.
7. Durst, F., Melling, A., and Whitelaw, J. H. 1976 "Principles and Practice of Laser-Doppler Anemometry ", Acad. Press N.Y.
8. Durst, F. and Stevenson, W. H. 1970 "Influence of Gaussian Beam Properties on Laser Doppler Signals", Appl. Optics, 18, No. 4, pp. 516-523.
9. East, L. F., and Sawyer, W. G. 1979 "An Investigation of the Structure of Equilibrium Turbulent Boundary Layers", Proc. of the NATO-AGARD Symposium.
10. Echols, W. H. and Young, J. A. 1963 "Studies of Portable Air-Operated Aerosol Generator", NBL 5929, July 29, 1963.
11. Kiland, R. 1979 Private Communications.
12. Kline, S. J. and McClintock, F. A. 1953 "Describing Uncertainties in Single-Sample Experiments", Mechanical Engineering, 75, pp. 3-8.
13. Kreid, D. K. and Grams, G. W. 1976 "Confocal LDV Utilizing a Decoupling Beam Splitter-Combiner", Appl. Optics, 15, pp. 14-16.
14. Miller, J. A. 1976 "Simple Linearized Hot-wire Anemometer", J. Fluids Engineering, 98, pp. 550-557.
15. Orloff, K. L. and Logan S. E. 1973 "Confocal Backscatter Laser Velocimeter with on-axis Sensitivity", Appl. Optics, 12, No. 10, pp. 2477-2481.

16. Sandborn, V. A. and Slogar, R. J. 1955 "Study of the Momentum Distribution of Turbulent Boundary Layers in Adverse Pressure Gradients", NACA TN 3264.
17. Schubauer, G. B. and Klebanoff, P. S. 1950 "Investigation of Separation of the Turbulent Boundary Layer", NACA TN 2133.
18. Simpson, R. L. and Wallace, D. B. 1975 "Laminariscient Turbulent Boundary Layers: Experiments on Sink Flows", Project SQUID Report SMU-1-PU.
19. Simpson, R. L. and Collins, M. A. 1978 "Prediction of Turbulent Boundary Layers in the Vicinity of Separation", AIAA Journal, 16, pp. 289-290.
20. Simpson, R.L. and Chew, Y.T. 1979 "Measurements in Highly Turbulent Flows: Steady and Unsteady Separated Turbulent Boundary Layers". Third Int. Workshop on Laser Velocimetry, Purdue Univ., July 1-13, 1978; Laser Velocimetry and Particle Sizing, H.D. Thompson and W.H. Stevenson, ed., pp. 179-196, Hemisphere, N.Y.
21. Simpson, R. L. 1979 "A Review of Some Phenomena in Turbulent Flow Separation", Project SQUID, Technical Report SMU-3-PU, Colloquium on Flow Separation, Jan. 1979.
22. Simpson, R. L., Heizer, K. W., and Nasburg, R. E. 1979 "Performance Characteristics of a Simple Linearized Hot-wire Anemometer", J. Fluids Engineering, 101, pp. 381-382.
23. Simpson, R. L., Chew, Y. -T., and Shivaprasad, B. G. 1980 "Measurements of a Separating Turbulent Boundary Lyaer", Project SQUID Report SMU-4-PU.
24. Strickland, J. H. and Simpson, R. L. 1973 "The Separating Turbulent Boundary Layer: An Experimental Study of an Airfoil Type Flow", Thermal and Fluid Sciences Center, Southern Methodist University, Report WT-2; also AD-771170/8GA.
25. Watrasiewichz, B. M. and Rudd, M. L. 1976 Laser Doppler Measurements Butterworths, London.
26. Wagnanski, I. and Fiedler, H. E. 1970 "The Two-dimensional Mixing Region", J. Fluid Mech., 41, pp. 327-361.

APPENDIX

TABULATED LASER
AND HOT-WIRE
ANEMOMETER DATA

X=115.500 INCHES

DATE: 3-9-80
MARQA

L.D.V. MEASUREMENTS

V (INS.)	W (F.P.S.)	ω^2 (F.P.S. ²)	S_ω	E_ω	ζ_ω
.010	-.11	3.62	.14	4.65	.43
.020	-.30	5.57	.07	3.74	.42
.030	-.20	5.74	.04	3.33	.43
.040	.65	6.65	.02	3.11	.59
.050	1.10	6.99	-.02	3.44	.48
.060	-.35	7.90	.14	3.17	.45
.080	.91	7.44	.16	3.06	.62
.100	2.77	7.75	.09	3.02	.84
.300	2.57	9.73	.20	3.17	.81
.500	-.58	10.06	.12	3.23	.38
.700	-.57	11.16	.10	3.79	.38
.900	.01	11.06	.20	3.12	.45
1.100	-.23	10.74	.08	3.27	.42
1.300	-.78	10.22	.14	3.20	.35
1.500	-.75	7.78	.10	3.36	.41
1.900	.16	6.06	.05	3.52	.50
2.300	-.26	2.95	-.24	4.47	.40
2.800	.06	.46	N.A.	N.A.	.44 (F.S.)

X=115.500 INCHES

DATE: 3-9-80
MAPOR

L.D.V. MEASUREMENTS

V (INS.)	W (F.P.S.)	ω^2 (F.P.S. ²)	S_ω	E_ω	ζ_ω
.010	-.09	3.93	.10	4.29	.44
.020	.74	5.40	.13	3.87	.50
.030	-.27	5.10	.08	3.43	.42
.030	-.88	6.35	.20	3.37	.31
.040	-.11	6.57	.19	3.22	.44
.050	.15	7.27	.05	3.00	.49
.060	.48	7.09	.23	3.55	.53
.070	.48	7.61	.16	3.32	.54
2.800	.13	.47	.06	8.33	.53 (F.S.)

X=119.670 INCHES

DATE: 1-30-80
JAN30A

L.D.V. MEASUREMENTS

V (INS.)	W (F.P.S.)	ω^2 (F.P.S. ²)	S_ω	E_ω	ζ_ω
.010	-.65	.64	-.16	2.83	.16
.010	-.36	.91	-.46	3.13	.36
.010	-.40	.42	-.14	3.07	.20
.020	-.42	1.30	-.09	3.10	.35
.030	-.36	1.82	.09	2.46	.40
.050	-.25	4.89	.10	2.60	.41
.110	-1.19	9.72	.00	2.93	.37

V=139.670 INCHES

DATE: 2-7-90
FEB7AA

L.D.V. MEASUREMENTS

V (INS.)	W (F.P.S.)	W ² (F.P.S.) ²	S _w	F _w	Y _w
.050	1.91	3.61	-.54	3.14	.83
.070	1.80	4.97	-.20	3.17	.72
.100	1.14	8.28	-.01	2.70	.64
.200	.92	7.91	.04	2.58	.61
.300	2.07	9.34	-.16	2.75	.75
.500	2.01	8.66	-.15	2.76	.74
1.000	.95	11.19	.17	2.76	.59
1.000	1.16	10.62	.05	2.59	.62
1.500	1.11	12.47	.03	2.64	.61
2.000	.05	15.63	.04	2.59	.49
2.500	-.94	14.95	.01	2.53	.40
2.500	-.27	14.74	.07	2.53	.46
3.000	1.35	16.49	.05	2.50	.50
3.500	1.03	12.78	.07	2.54	.59
4.000	.78	11.94	.04	2.70	.51
4.500	.66	8.05	-.08	2.80	.58
5.000	-.58	6.15	-.27	2.97	.41
5.000	.61	5.51	-.13	2.64	.61
5.000	.99	6.17	-.09	2.76	.66
6.000	.02	.41	.45	2.97	.47
6.000	.35	.44	-.18	2.47	.67
7.000	-.32	.22	-.02	2.60	.24
7.000	-1.01	.24	-.01	2.67	.01
7.000	-.22	.18	.19	2.51	.28

(F.S.)

V=139.670 INCHES

DATE: 2-12-90
FEB12A

L.D.V. MEASUREMENTS

V (INS.)	W (F.P.S.)	W ² (F.P.S.) ²	S _w	F _w	Y _w
.010	-.13	.08	-.40	2.96	.30
.070	.11	.04	-.35	2.62	.68
.070	-.43	.41	-.50	2.23	.24
.030	-.47	2.54	-.09	2.96	.33
.050	-.44	5.70	-.63	3.49	.44
.100	-.59	9.67	-.34	2.97	.42
.500	.17	7.45	-.02	2.64	.50
1.000	-.51	10.14	-.22	2.75	.44
1.000	.01	11.02	-.05	2.63	.49
2.000	-.66	12.89	-.04	2.56	.42
2.500	-1.09	14.30	-.22	2.92	.38
2.500	-.04	14.32	-.11	2.59	.49
2.800	.11	14.37	.01	2.96	.48
4.000	-.88	11.08	-.10	2.65	.40
5.000	-1.70	4.39	-.57	3.46	.18
7.000	.01	.26	.15	3.01	.48

(F.S.)

X=140.330 INCHES

DATE: 3-31-80
MAR 31A

L.D.V. MEASUREMENTS

Y (INS.)	W (F.P.S.)	W ² (F.P.S. ²)	S _w	F _w	Y _w
.040	-.33	.35	N.A.	N.A.	.04
.060	-.35	.90	-.69	6.80	.13
.200	-.47	6.84	-.09	3.91	.28
.400	1.87	9.94	.09	2.99	.68
.600	1.12	9.28	.02	2.85	.58
1.100	-1.19	9.44	.06	2.84	.30
1.600	.36	15.24	.15	2.87	.44
2.100	1.98	17.32	.09	3.14	.50
2.600	.64	19.81	-.04	3.04	.48
3.100	.21	22.97	.01	3.00	.44
4.100	.62	28.84	.00	2.83	.48
4.600	.90	31.92	.17	3.46	.50
5.100	-.29	35.95	-.04	2.87	.43
5.600	-.01	34.05	-.01	2.92	.45
6.100	-.41	35.39	.04	2.89	.42
6.600	.46	36.36	.03	2.97	.48
7.100	1.60	33.32	-.07	3.15	.56
7.600	.13	28.68	-.09	3.09	.53
8.100	-.17	22.55	.09	3.94	.40
8.600	-1.11	9.36	.00	4.08	.29
9.100	.13	5.27	-.46	4.83	.57
9.600	.64	2.41	-.32	4.49	.60
9.600	1.13	2.11	-.03	3.48	.73
10.100	.64	1.11	.14	3.59	.68
10.750	-.27	.60	.01	3.02	.29
10.750	-.80	.38	-.21	3.28	.09 (F.S.)

X=173.250 INCHES

DATE: 3-26-80
MAR 26A

L.D.V. MEASUREMENTS

Y (INS.)	W (F.P.S.)	W ² (F.P.S. ²)	S _w	F _w	Y _w
.075	-.05	.42	.69	7.88	.51
.090	-.06	5.88	.02	4.17	.37
.400	.02	11.22	.05	2.81	.46
.570	-.02	11.60	.07	2.94	.47
1.400	1.13	11.65	-.06	3.07	.64
1.900	.20	12.84	.01	3.28	.49
2.400	-.55	14.04	-.19	3.24	.41
3.000	.71	15.71	-.02	3.10	.54
3.400	1.40	16.53	.02	2.91	.60
3.900	.73	20.70	.03	3.07	.53
4.400	-.11	22.10	.01	2.96	.51
4.470	.28	25.11	.03	2.94	.46
4.900	1.03	27.51	.05	2.96	.57
5.400	.50	29.37	.00	2.93	.48
5.900	1.13	33.52	-.03	2.84	.57
6.400	.32	33.05	-.02	2.79	.46
6.900	.72	36.71	-.03	2.88	.55
7.300	.37	39.08	.08	2.77	.50
7.900	-1.00	39.80	.00	2.88	.39
8.400	-.69	37.59	.06	2.87	.45
8.900	-.37	38.16	.00	2.93	.42
9.400	.15	35.10	.06	2.95	.45
9.900	1.84	34.00	.05	3.02	.57
10.700	-1.21	33.53	.00	3.11	.36
10.900	-.36	21.80	-.34	3.51	.41
11.400	-.34	15.65	.05	4.34	.34
11.900	.87	12.51	-.29	4.12	.55
12.400	.27	3.71	-.44	6.74	.50
12.470	-.57	4.93	-.29	6.41	.31
12.900	-.14	1.79	.10	4.99	.35

X=139.670 INCHES

DATE: 3- 5-60

HOT-WIRE (X-WIRE) MEASUREMENTS

Y (INS.)	U (F.P.S.)	U^2 (F.P.S.) ²	W^2 (F.P.S.) ²	$-UW$ (F.P.S.) ²
4.000	33.37	29.29	12.52	-1.62
4.300	36.52	24.52	10.50	-1.98
4.600	39.54	16.89	7.45	-1.01
4.900	42.30	9.73	4.65	-1.16
5.200	44.41	2.06	2.64	-.46
5.500	45.72	N.A.	1.22	-.43
6.000	46.03	.15	N.A.	-.03
7.100	46.06	N.A.	N.A.	-.03

(F.S.)

X=160.330 INCHES

DATE: 3-11-60

HOT-WIRE (X-WIRE) MEASUREMENTS

Y (INS.)	U (F.P.S.)	U^2 (F.P.S.) ²	W^2 (F.P.S.) ²	$-UW$ (F.P.S.) ²
7.500	29.25	47.32	14.74	-.22
8.000	33.70	42.90	12.81	-1.26
9.500	37.24	31.58	7.84	-.36
9.000	40.05	18.82	3.72	-.73
9.500	42.45	9.27	3.75	-.26
10.000	43.44	.48	1.61	.29
10.500	43.73	1.69	.37	-.17
13.000	43.87	.03	N.A.	-.02

(F.S.)

X=171.250 INCHES

DATE: 3- 7-60

HOT-WIRE (X-WIRE) MEASUREMENTS

Y (INS.)	U (F.P.S.)	U^2 (F.P.S.) ²	W^2 (F.P.S.) ²	$-UW$ (F.P.S.) ²
10.500	34.02	44.47	14.06	-.52
11.000	36.76	36.24	10.11	-2.30
12.500	38.70	24.74	5.95	.28
12.000	40.61	19.16	2.76	-.47
12.500	41.99	9.25	.03	-.56
13.500	42.93	N.A.	1.16	-.23

(F.S.)

09.01.11.UCLP. 13.

0.450 XLNS. ACX0017A UCTD. 05.

0.008 KP6S.

X= 67.813 INCHES

DATE: 3-19-80

HOT-WIRE (X-WIRE) MEASUREMENTS

Y (INS.)	U (F.P.S.)	U^2 (F.P.S.) ²	ω^2 (F.P.S.) ²	$-\frac{U\omega}{2}$ (F.P.S.) ²	
.050	46.33	29.83	8.53	.23	
.080	48.94	28.96	8.07	.09	
.120	51.51	27.06	7.53	-.02	
.160	53.83	24.99	7.19	.06	
.200	55.64	23.75	6.64	-.02	
.240	57.39	20.77	6.72	-.02	
.320	60.34	17.06	5.16	-.18	
.400	62.70	13.23	4.04	-.09	
.480	64.84	9.69	2.82	.12	
.560	66.71	6.91	1.88	-.02	
.640	68.14	4.35	1.04	.08	
.720	69.07	2.28	.39	.07	
.800	69.79	.87	N.A.	.05	
.940	70.45	N.A.	.06	.01	(F.S.)

X=115.500 INCHES

DATE: 2-26-80

HOT-WIRE (X-WIRE) MEASUREMENTS

Y (INS.)	U (F.P.S.)	U^2 (F.P.S.) ²	ω^2 (F.P.S.) ²	$-\frac{U\omega}{2}$ (F.P.S.) ²	F_w	S_w
.398	72.60	22.45	7.81	-.58	2.42	-.09
.523	74.78	23.15	8.85	-.59	2.61	-.04
.648	77.20	24.28	9.56	-.67	2.56	.03
.798	82.07	24.10	10.13	-.88	2.97	.05
1.148	86.62	21.50	9.60	-.51	2.86	.07
1.398	91.17	17.54	8.30	-.75	2.69	-.08
1.648	94.62	11.66	6.21	-.46	2.19	-.27
1.898	98.50	11.16	3.87	-.43	N.A.	-.77
2.148	91.27	5.11	1.54	-.06	N.A.	N.A.
2.398	92.83	1.17	.22	-.02	N.A.	N.A.

X=179.950 INCHES

DATE: 3-24-80

HOT-WIRE (X-WIRE) MEASUREMENTS

Y (INS.)	U (F.P.S.)	U^2 (F.P.S.) ²	ω^2 (F.P.S.) ²	$-\frac{U\omega}{2}$ (F.P.S.) ²	
1.800	30.38	29.73	12.30	-2.11	
2.150	35.60	23.68	10.53	-2.06	
2.350	38.19	20.75	9.34	-1.59	
2.550	40.83	16.02	7.57	-1.23	
2.750	43.90	11.32	4.18	-.46	
3.101	46.96	2.74	2.21	-.23	
3.450	49.43	1.34	.33	-.04	
3.800	49.22	N.A.	N.A.	-.01	
4.500	50.02	N.A.	N.A.	.00	(F.S.)

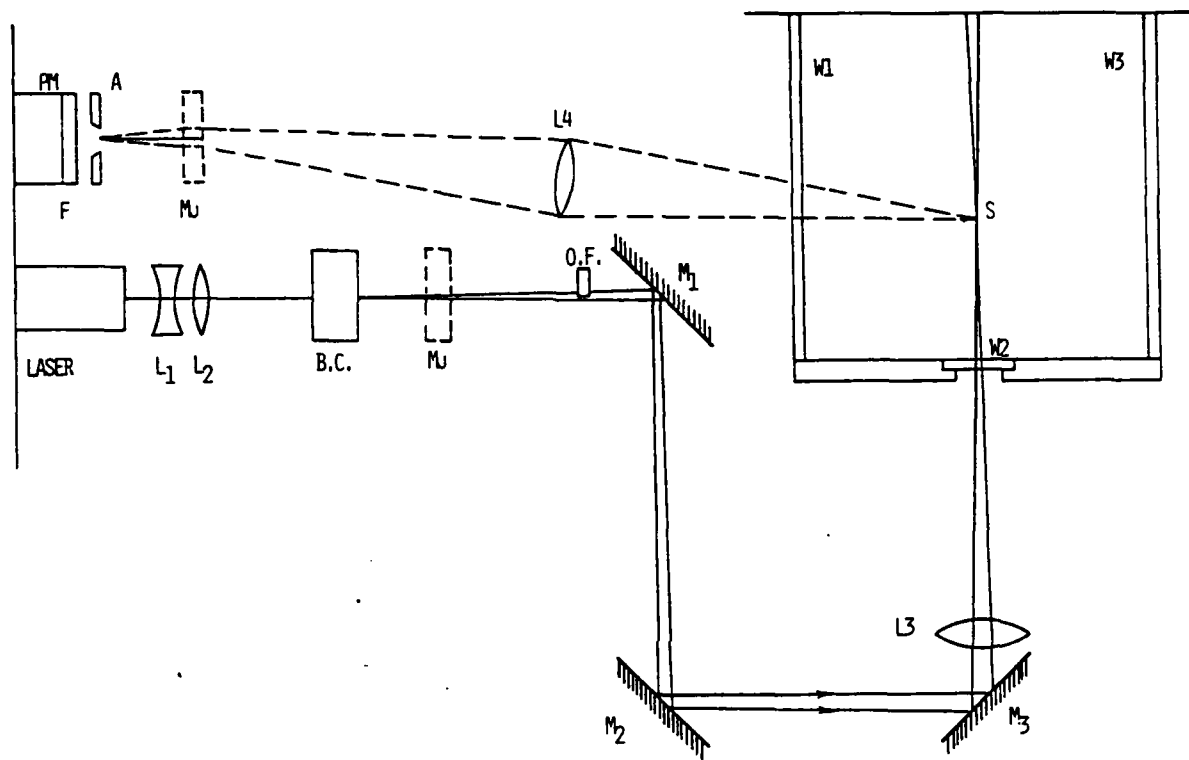


Figure 1. Sideview schematic of the fringe-type laser anemometer used to measure w . Key to component representation in Figures 1, 2, and 3:

- A - aperture, slit or iris
- B.C. - Bragg cell
- F - $0.488 \mu\text{m}$ wavelength filter
- L_i - lenses
- M_i - adjustable mirrors
- M_j - beam folding mirrors
- O.F. - optical flat
- P.M. - photomultiplier tube
- S - sampling volume

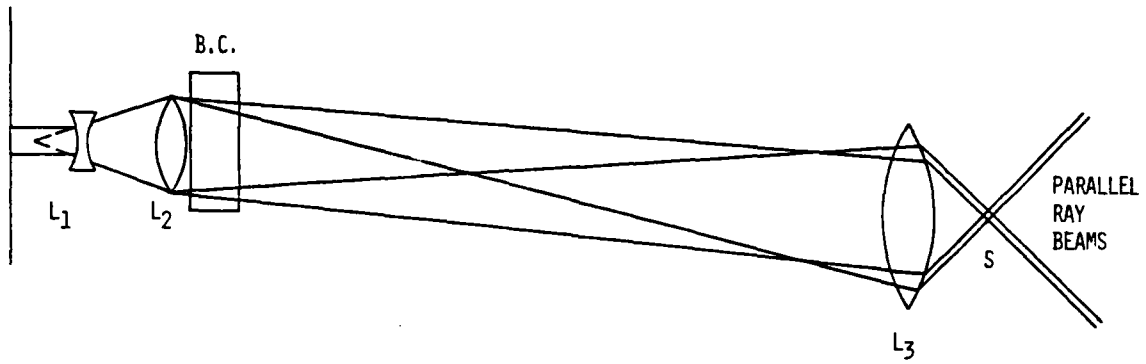


Figure 2. Sideview schematic of the optical components required to produce parallel ray beams at the beam crossing.

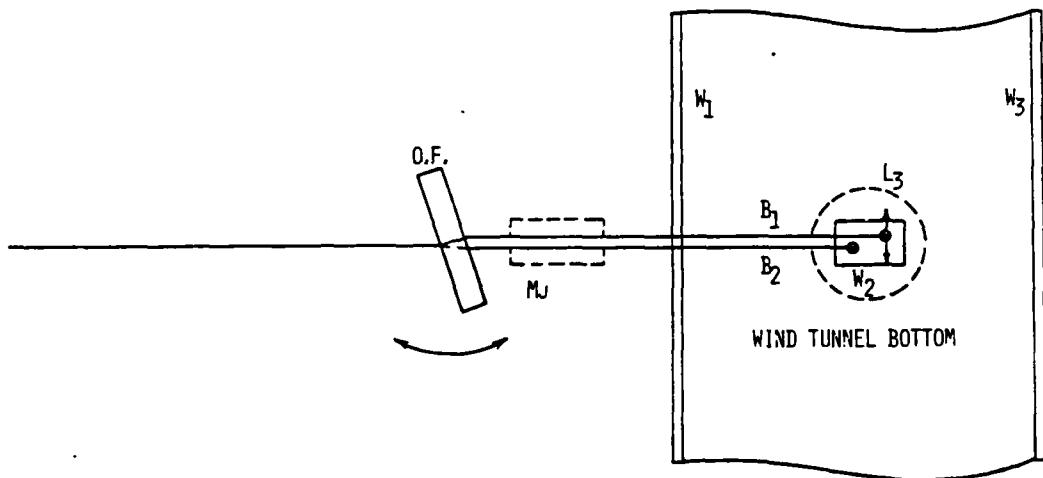


Figure 3. Schematic top view of the optical flat adjustment for beam alignment in the wind tunnel.



Figure 4. Photograph of the laser anemometer optics in the test position

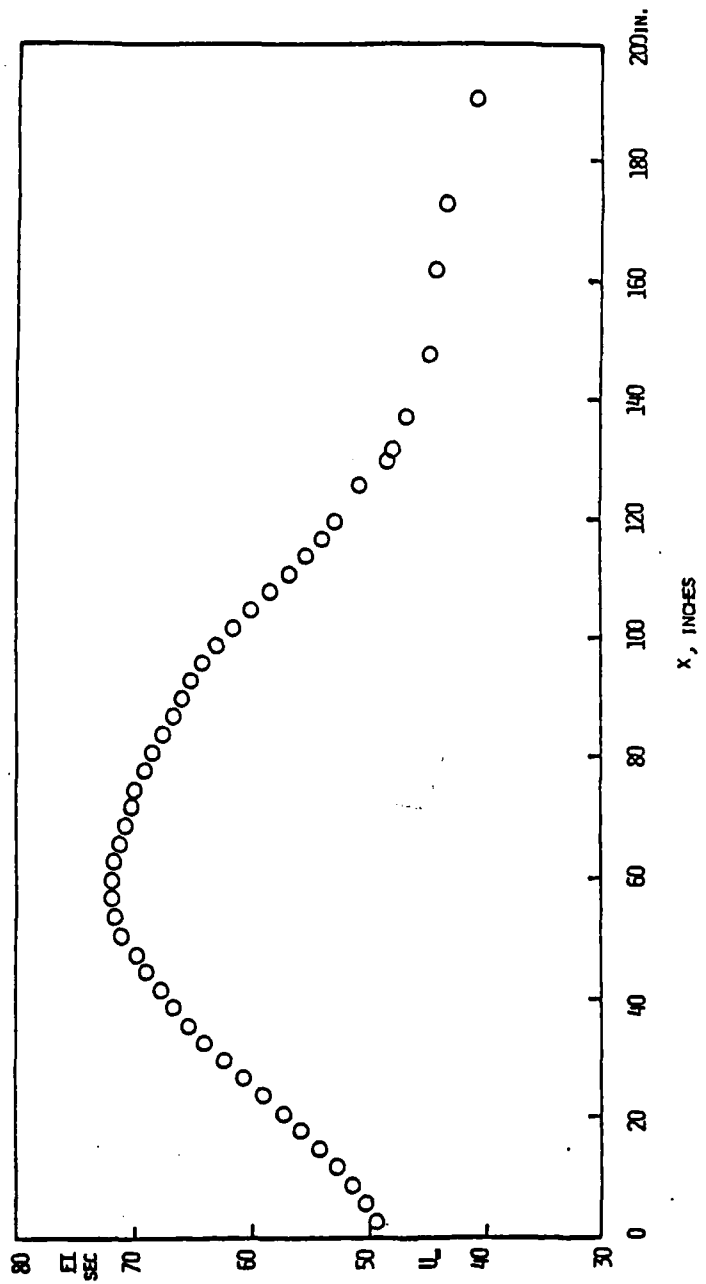


Figure 5. Freestream velocity distribution along the tunnel centerline.

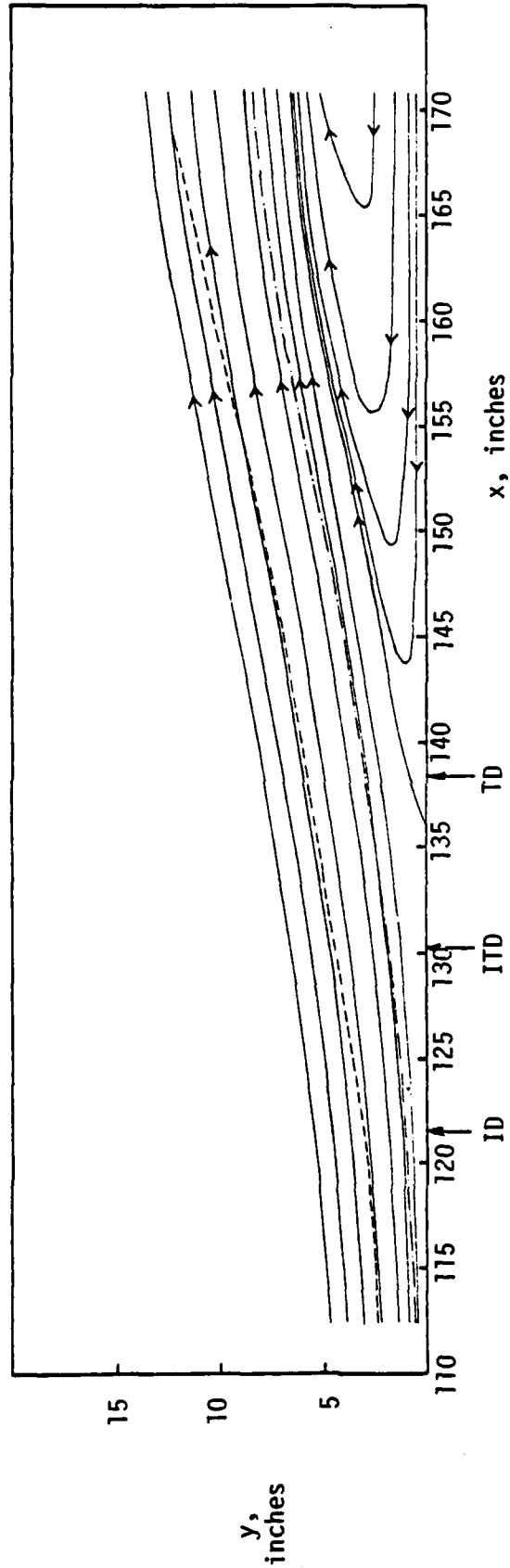


Figure 6. Mean streamline flow pattern in the vicinity of separation. — streamlines, - - - boundary layer edge, - - - displacement thickness distribution. ID denotes incipient detachment with 1% instantaneous backflow near the wall. ITD denotes intermittent transitory detachment with 20% instantaneous backflow near the wall. TD denotes transitory detachment with 50% instantaneous backflow near the wall.

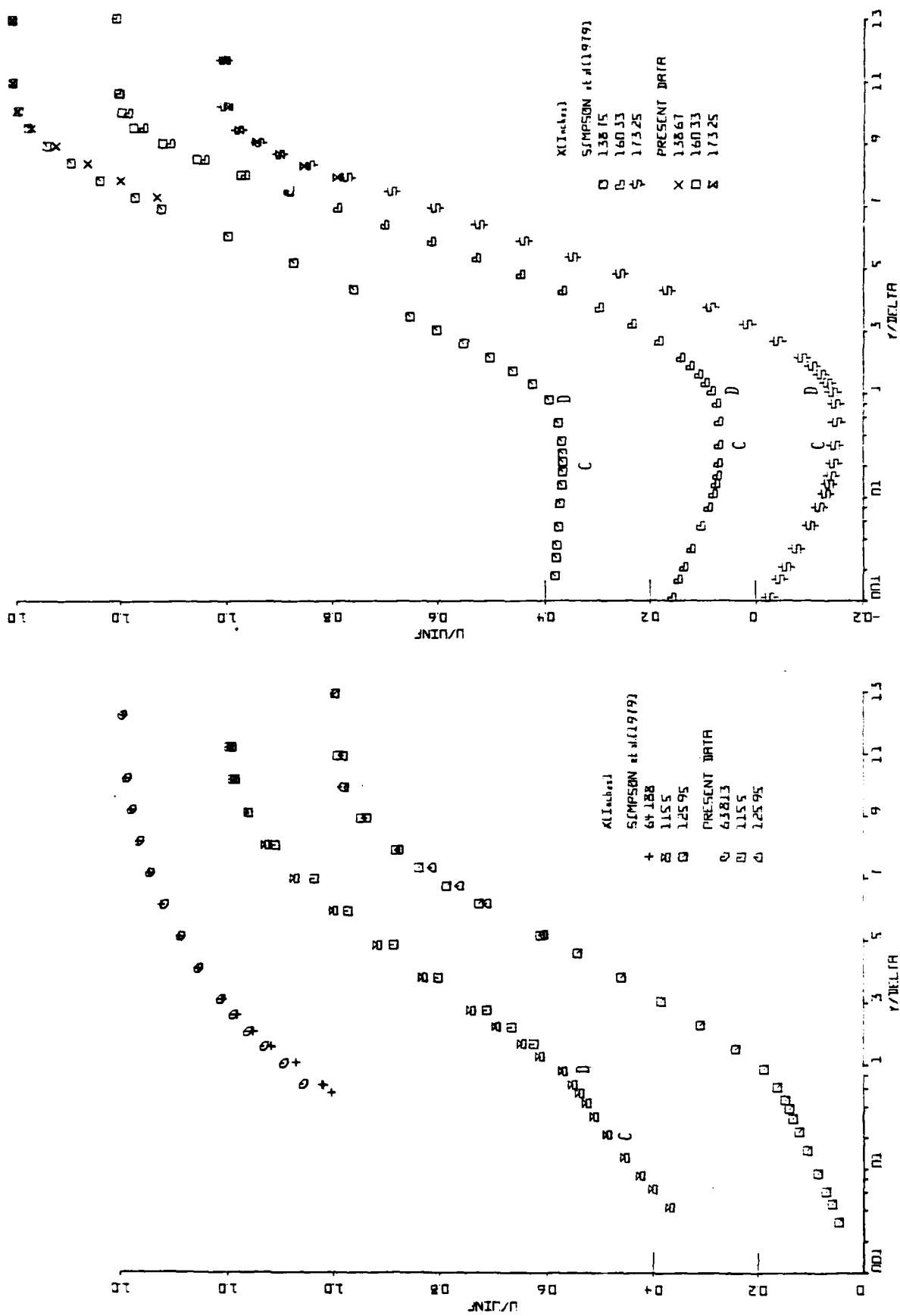


Figure 7. Mean velocity U/U_{∞} vs. y/δ profiles of present and previous data for this flow. Note displaced ordinates and the log-linear abscissa.

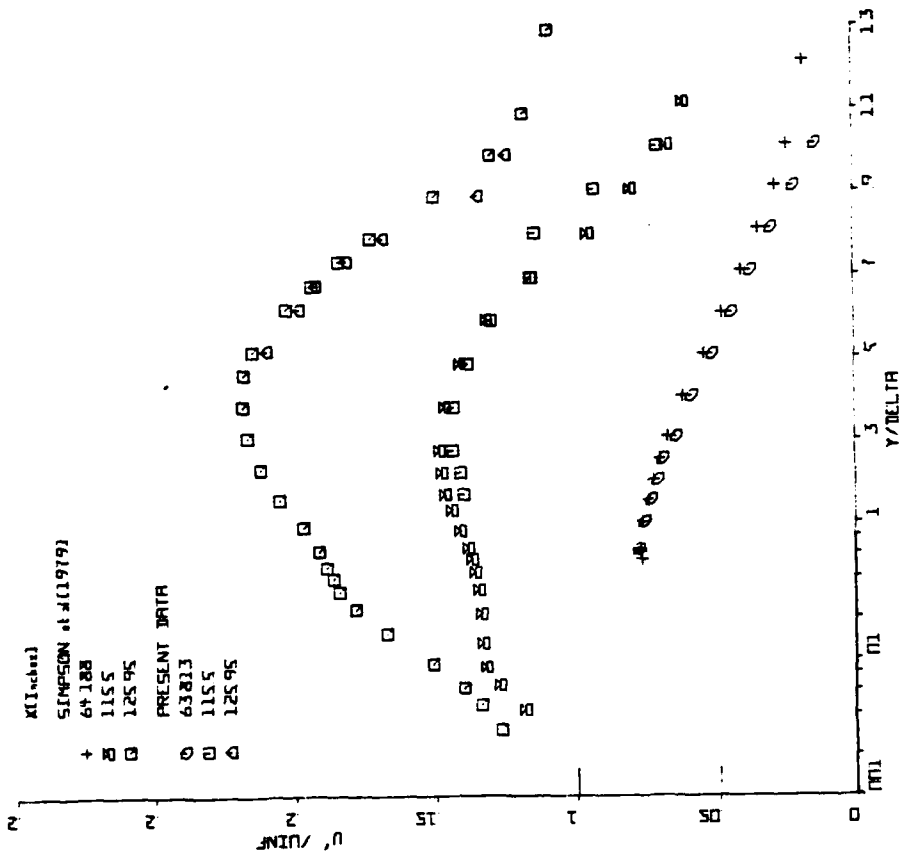
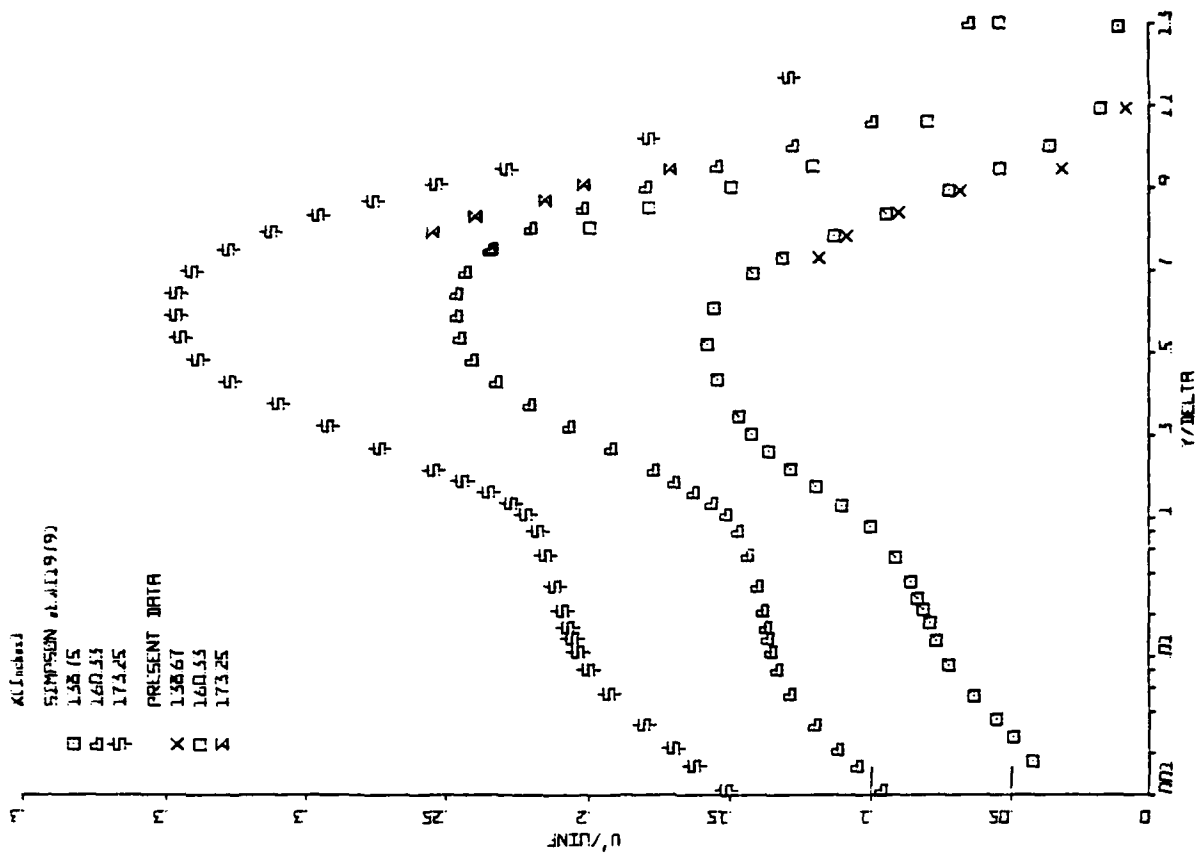


Figure 8. Turbulence intensity u' / U_{∞} vs. y / δ profiles of present and previous data for this flow. Note displaced ordinates and the log-linear abscissa.

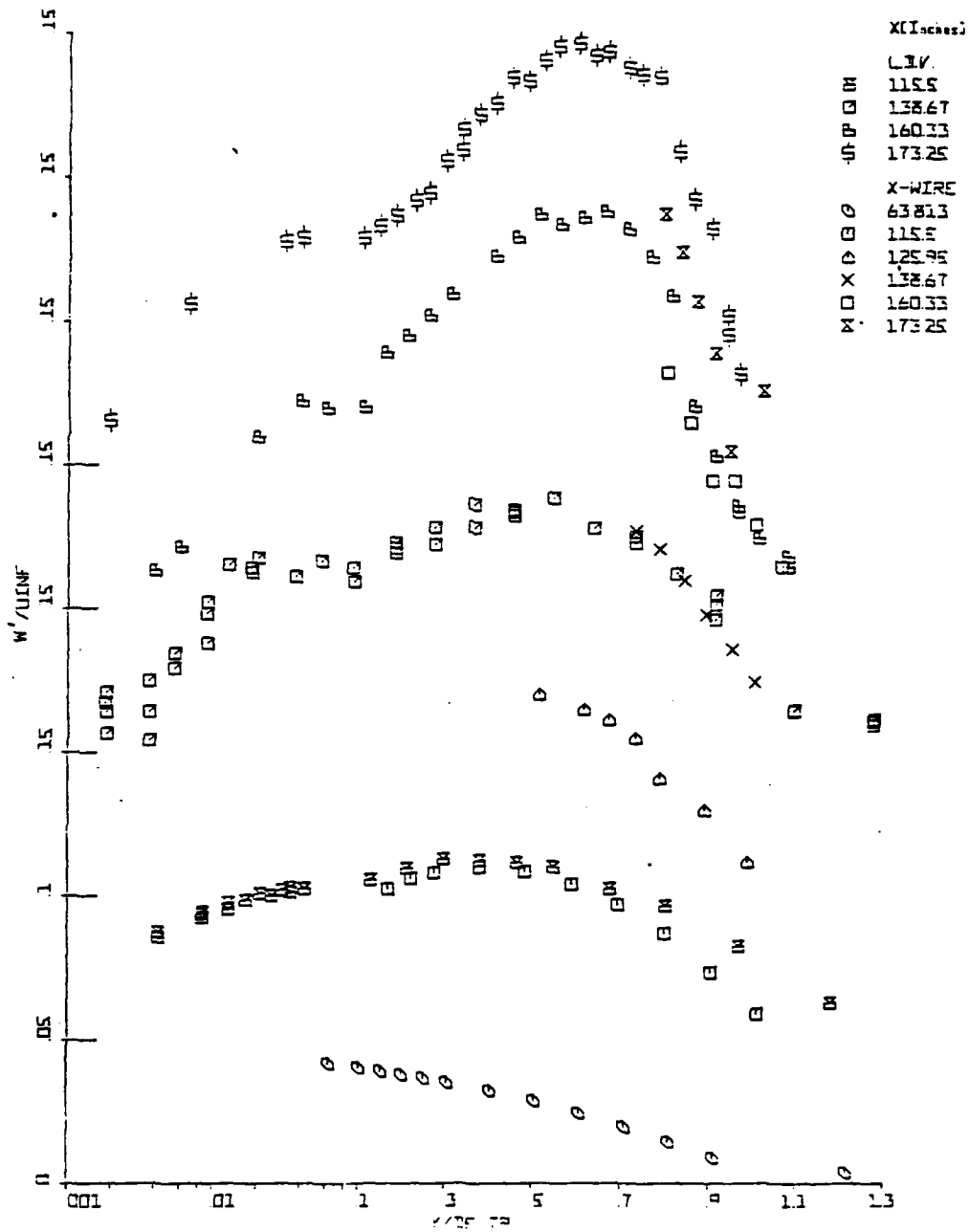


Figure 9. Profiles of laser and hot-wire anemometers results for w'/U_∞ . Note displaced ordinates and the log-linear abscissa.

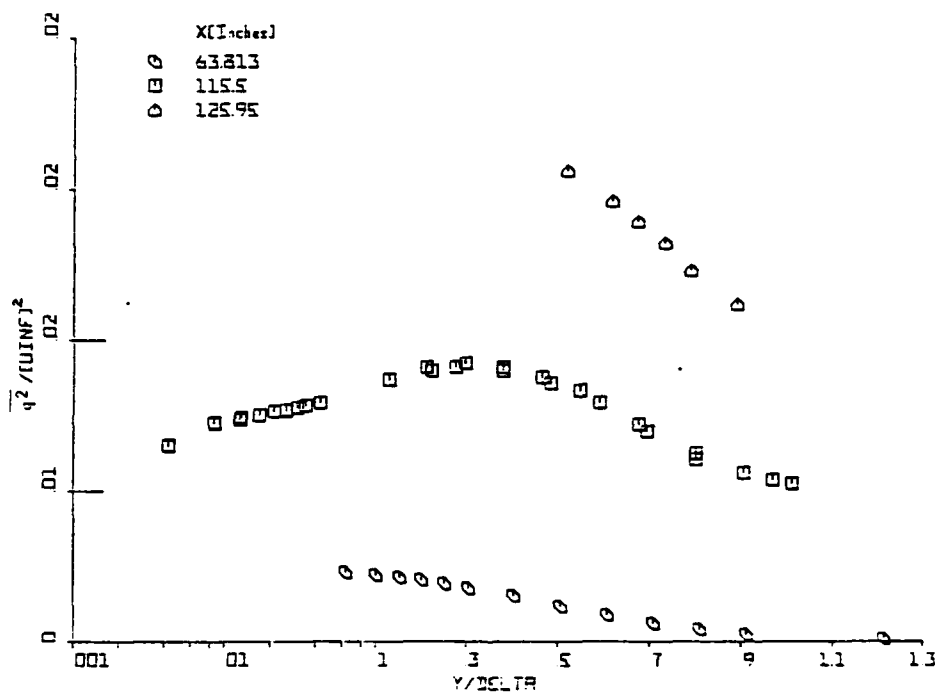


Figure 10(a). Non-dimensional turbulent kinetic energy distributions across the flow. Note displaced ordinates and the log-linear abscissa.

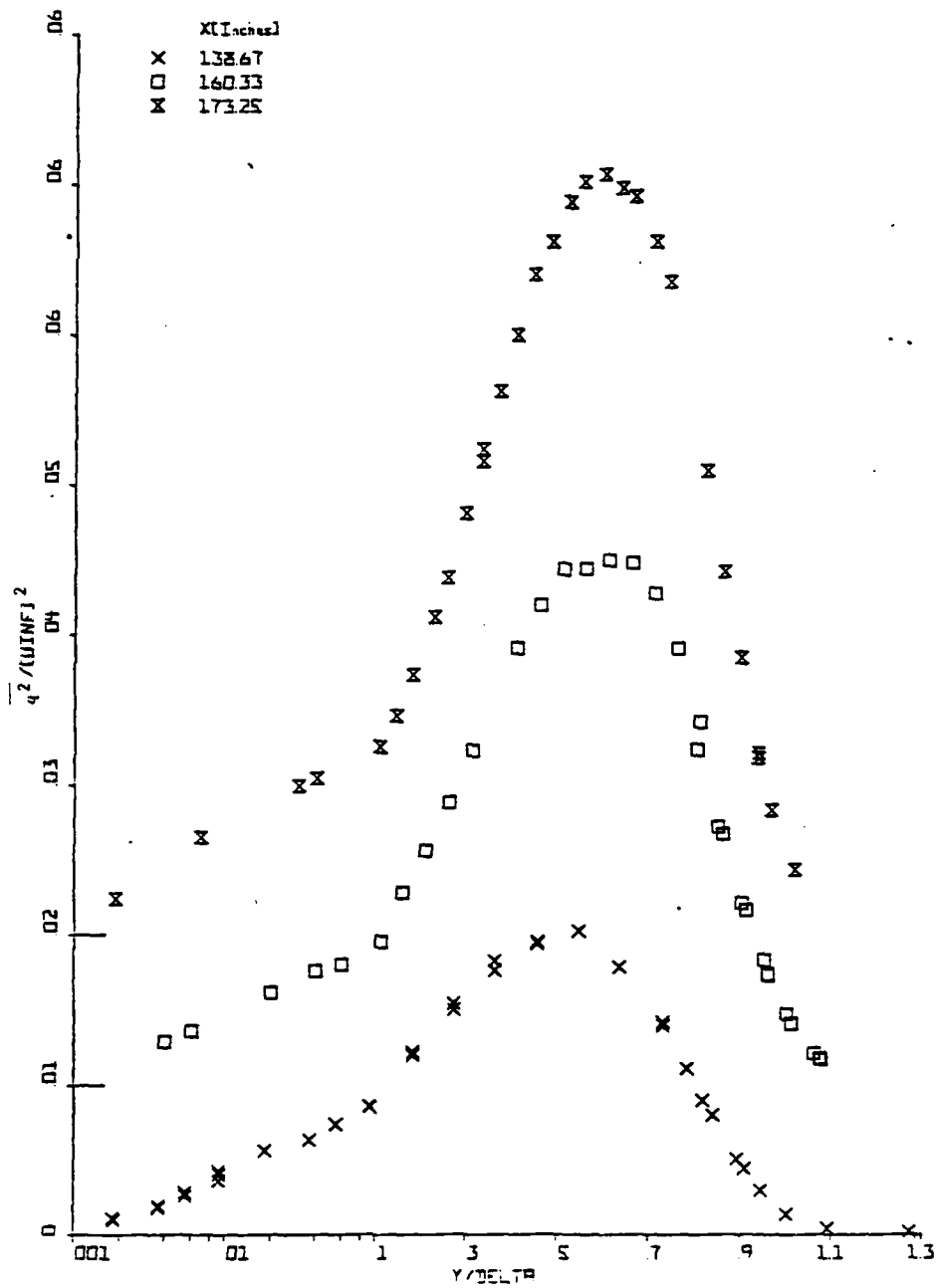


Figure 10(b). Non-dimensional turbulent kinetic energy distributions across the flow. Note displaced ordinates and the log-linear abscissa.

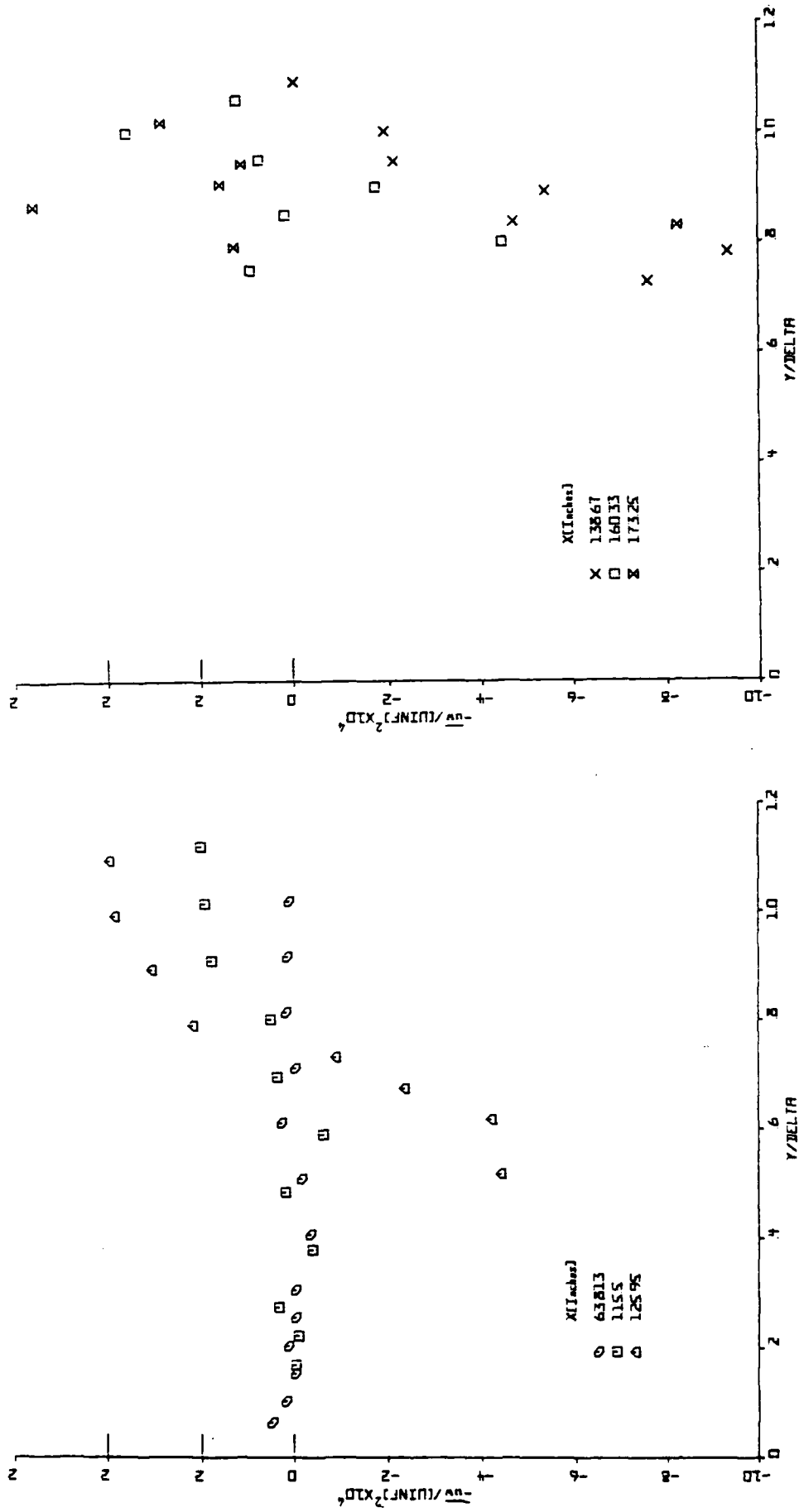


Figure 11. Non-dimensional $-\overline{u'w}/U_{\infty}^2$ vs. y/δ profiles. Note displaced ordinates and the log-linear abscissa.

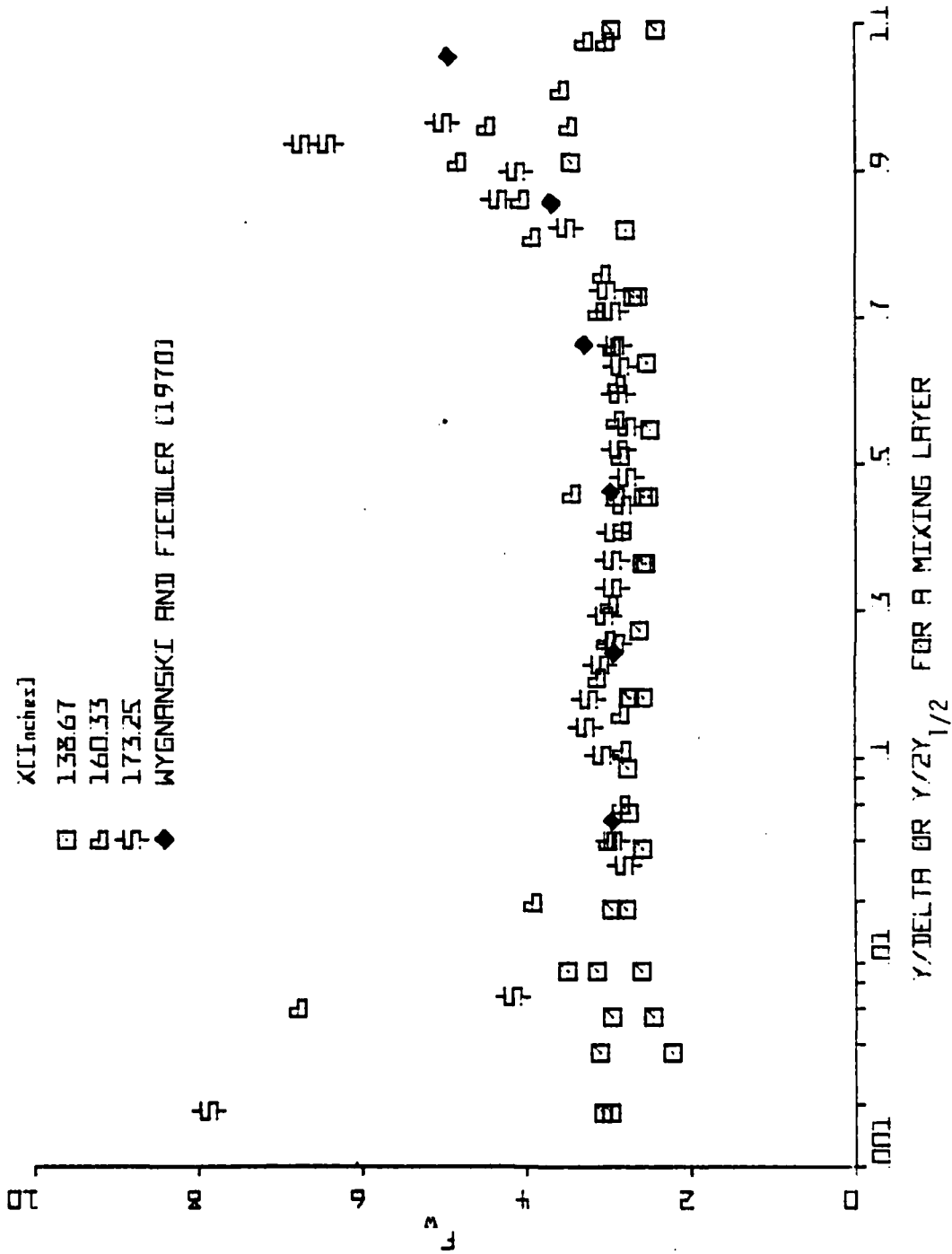


Figure 14. F_w from laser anemometer data downstream of separation. Note the log-linear abscissa.

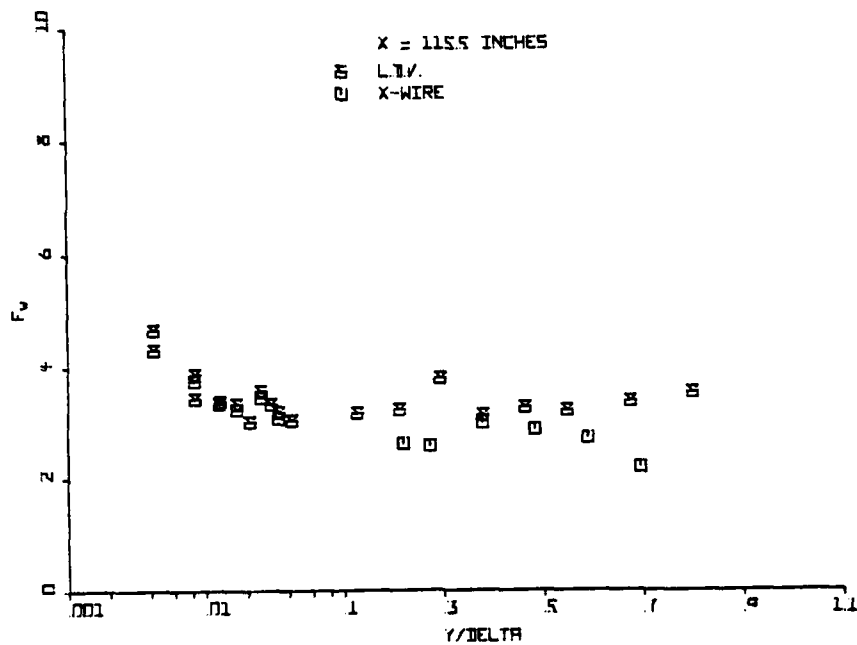


Figure 12. Comparison of laser and hot-wire anemometer results for the flatness factor F_w upstream of separation. Note log-linear abscissa.

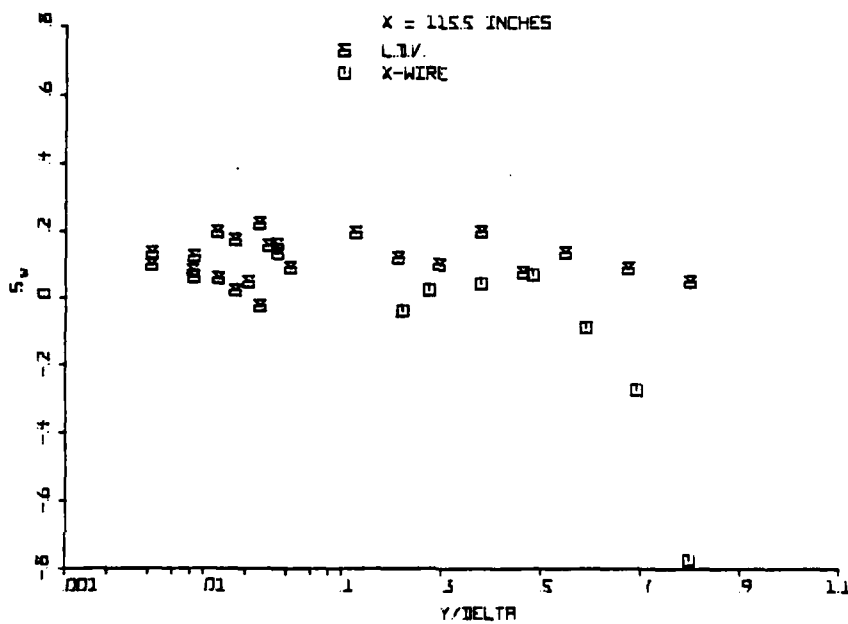


Figure 13. Comparison of laser and hot-wire anemometer results for the skewness factor S_w upstream of separation. Note the log-linear abscissa.

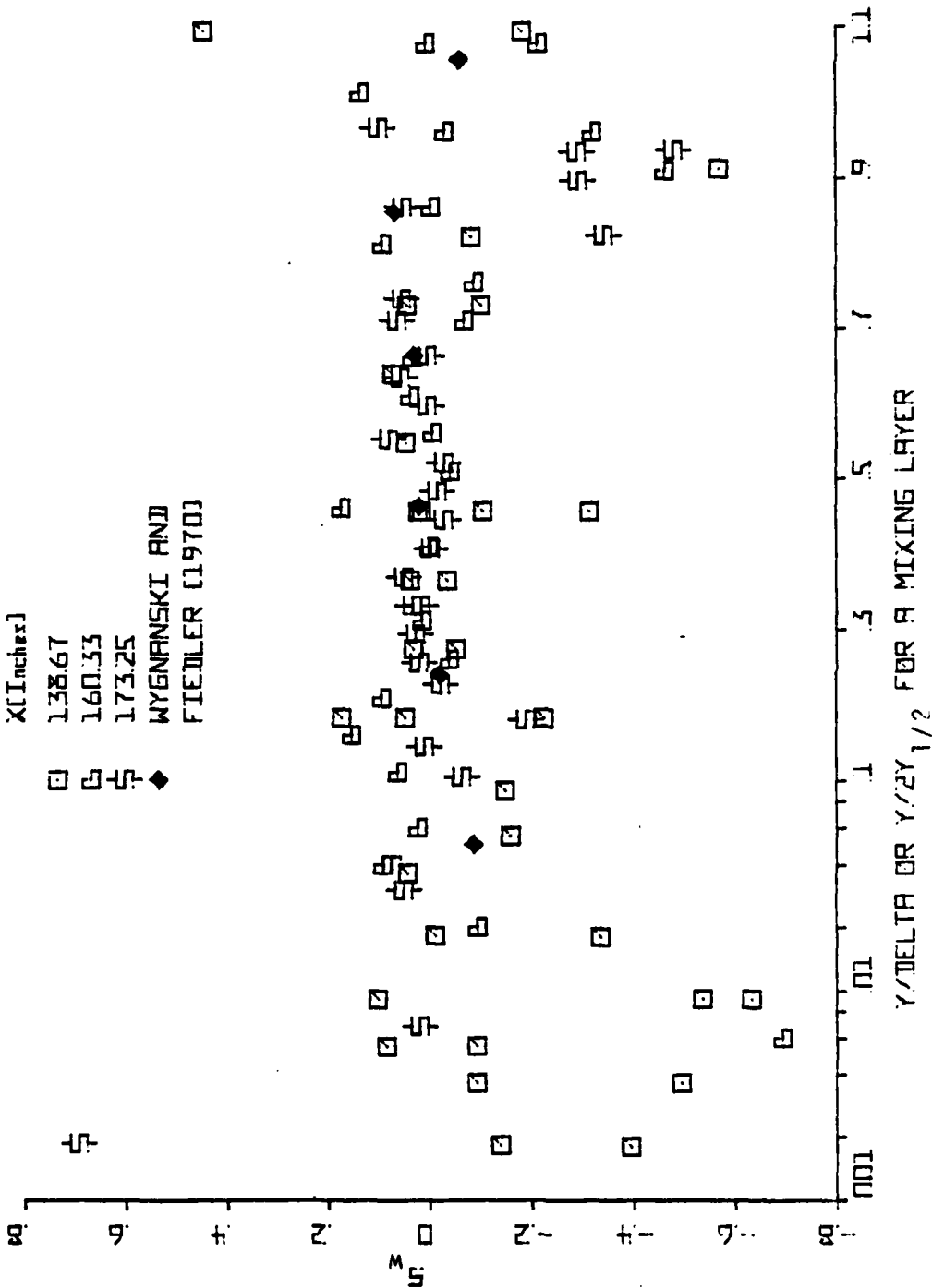


Figure 15. S_w from laser anemometer data downstream of separation. Note the log-linear abscissa.

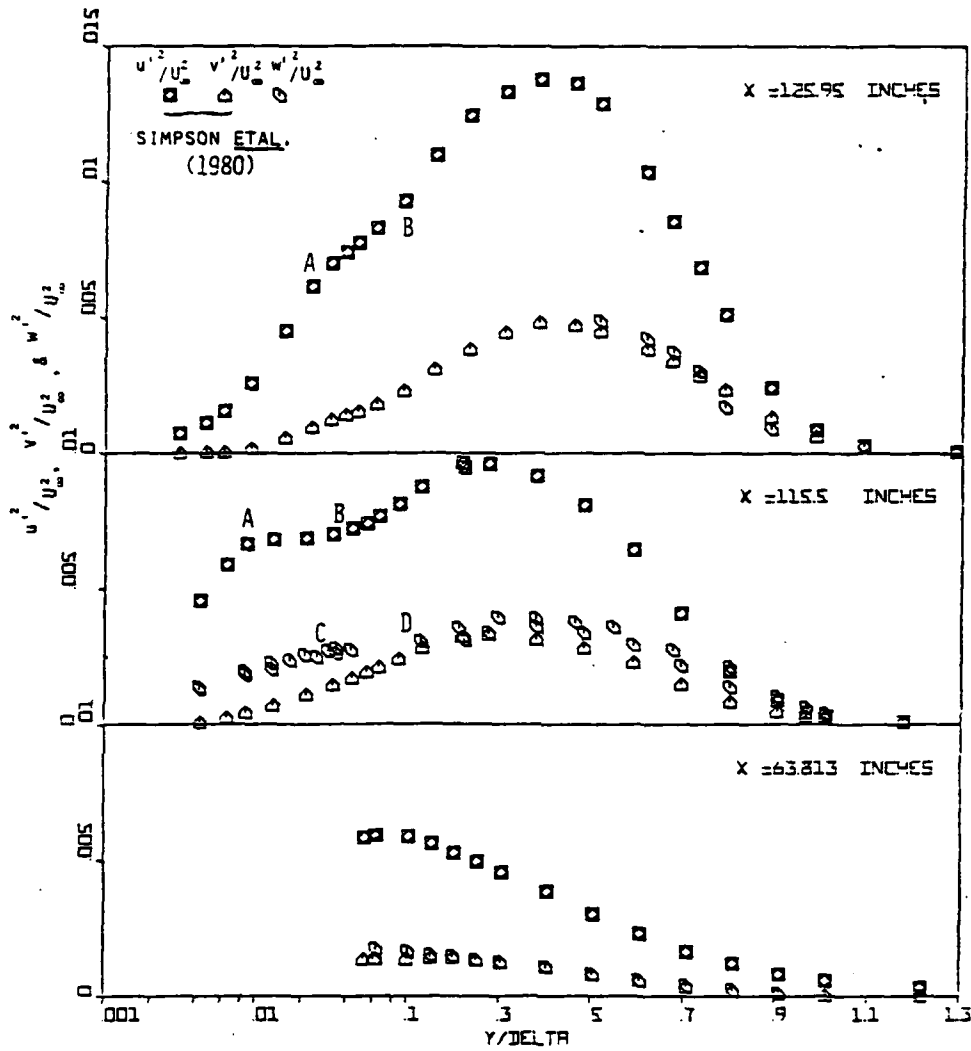


Figure 16(a). Non-dimensional $u'^2/U_\infty^2, v'^2/U_\infty^2, w'^2/U_\infty^2$ Reynolds stress distributions at each of the several streamwise locations. Note the log-linear abscissa.

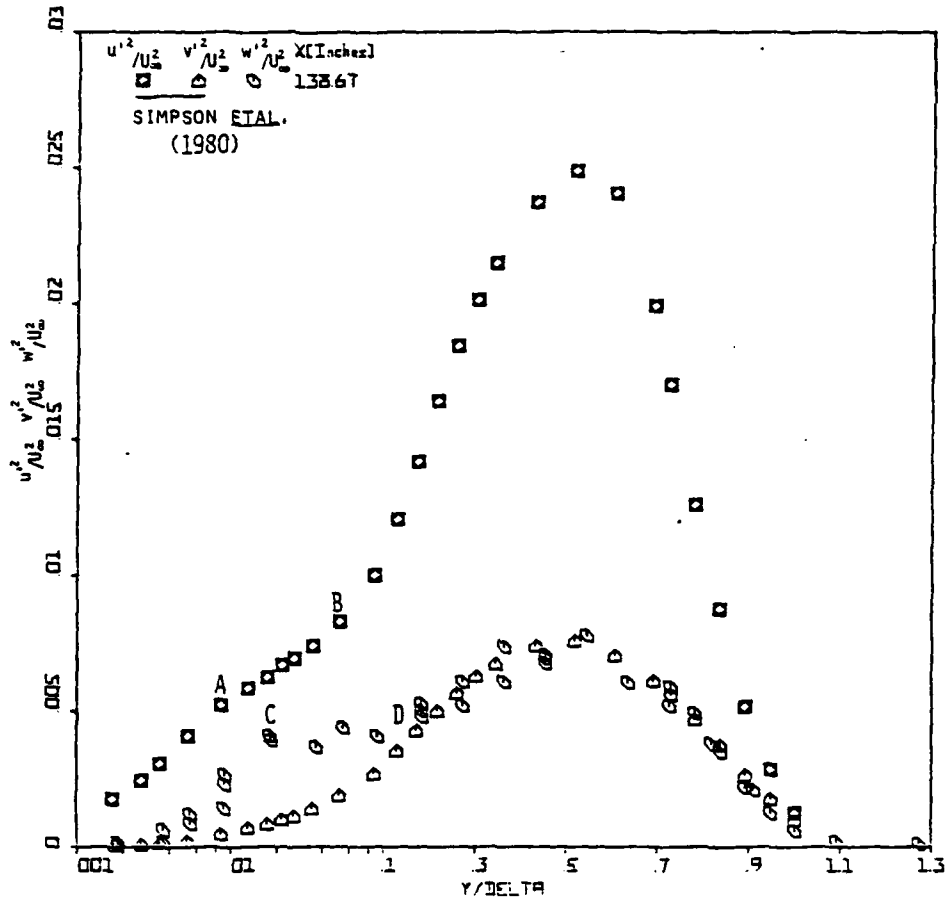


Figure 16(b). Non-dimensional $u'^2/U_\infty^2, v'^2/U_\infty^2, w'^2/U_\infty^2$ Reynolds stress distributions.

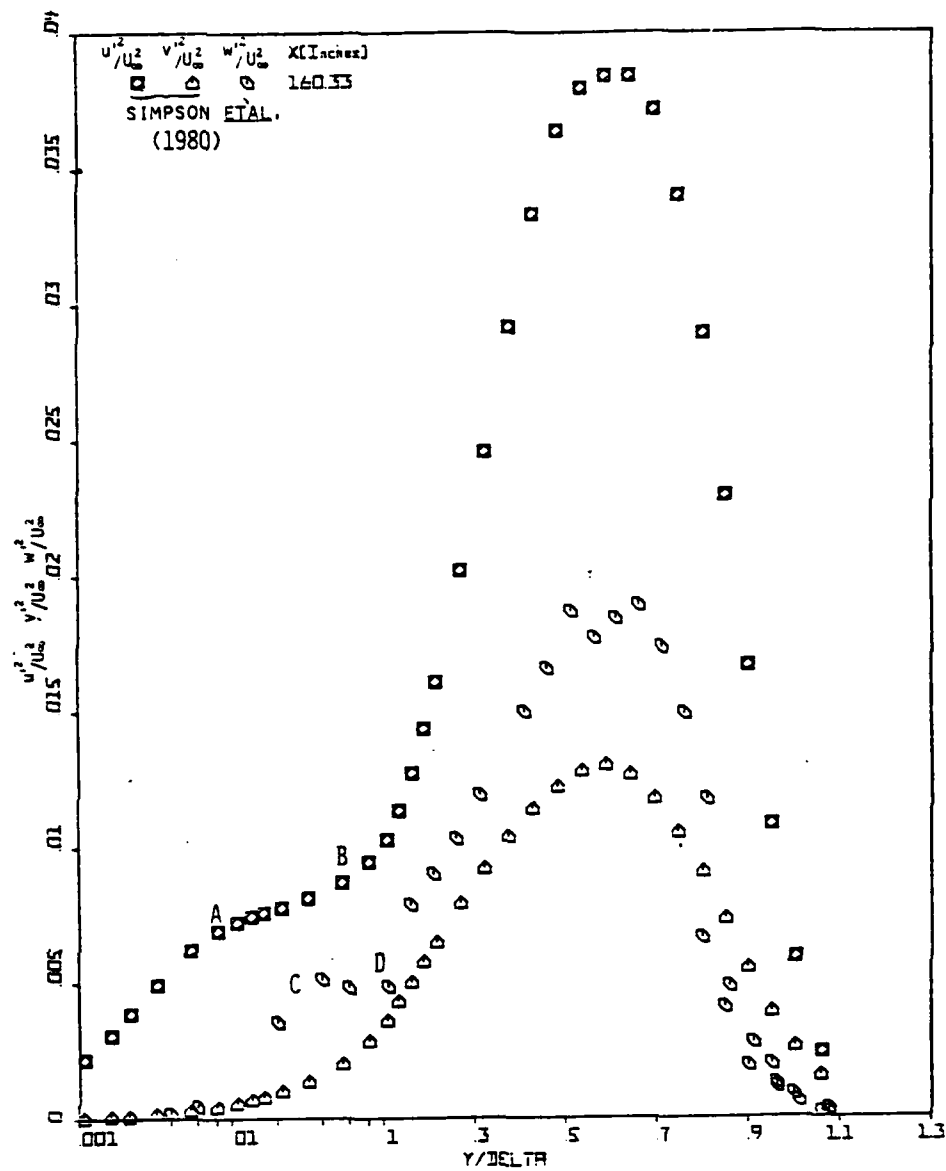


Figure 16(c). Non-dimensional $u'^2/U_\infty^2, v'^2/U_\infty^2$ Reynolds stress distributions.

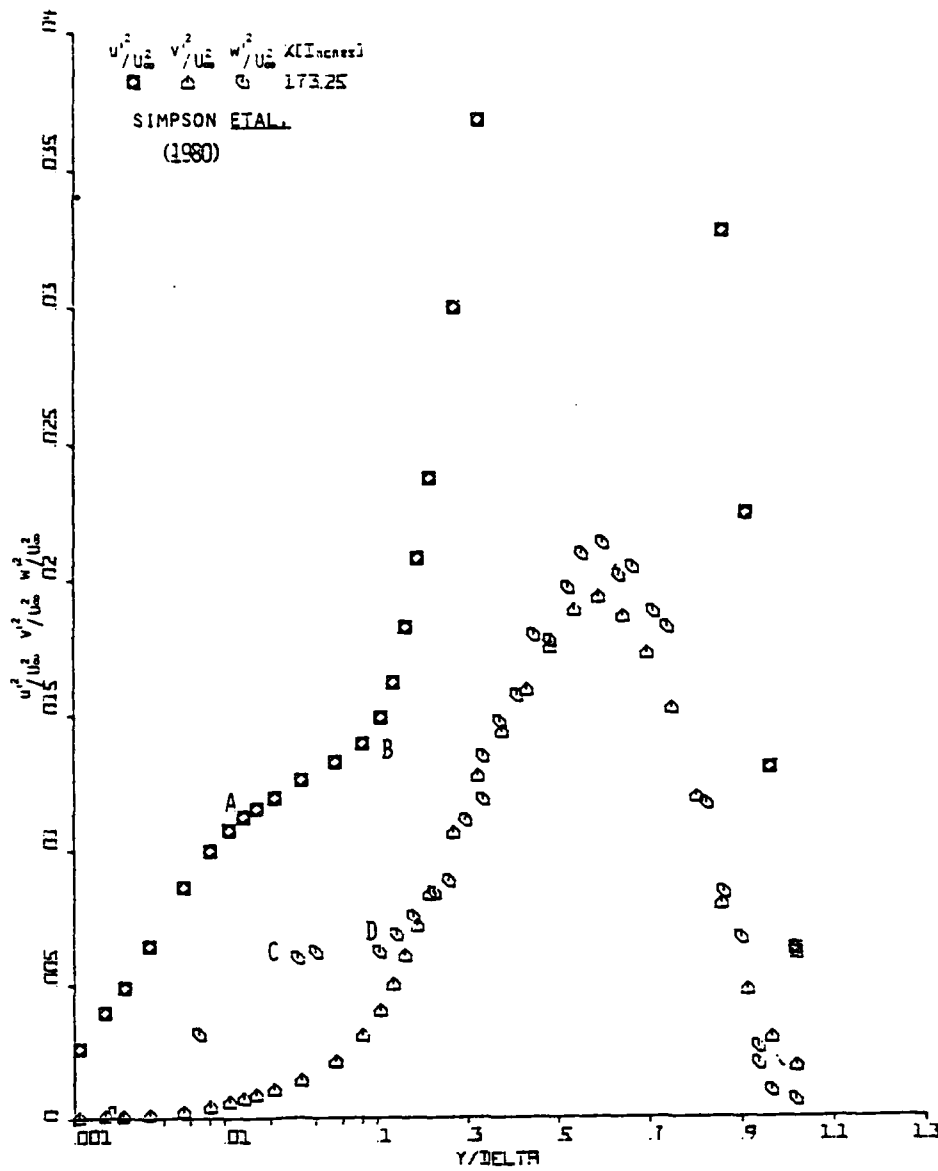


Figure 16(d). Non-dimensional $u'^2/U_\infty^2, v'^2/U_\infty^2$ Reynolds stress distributions.

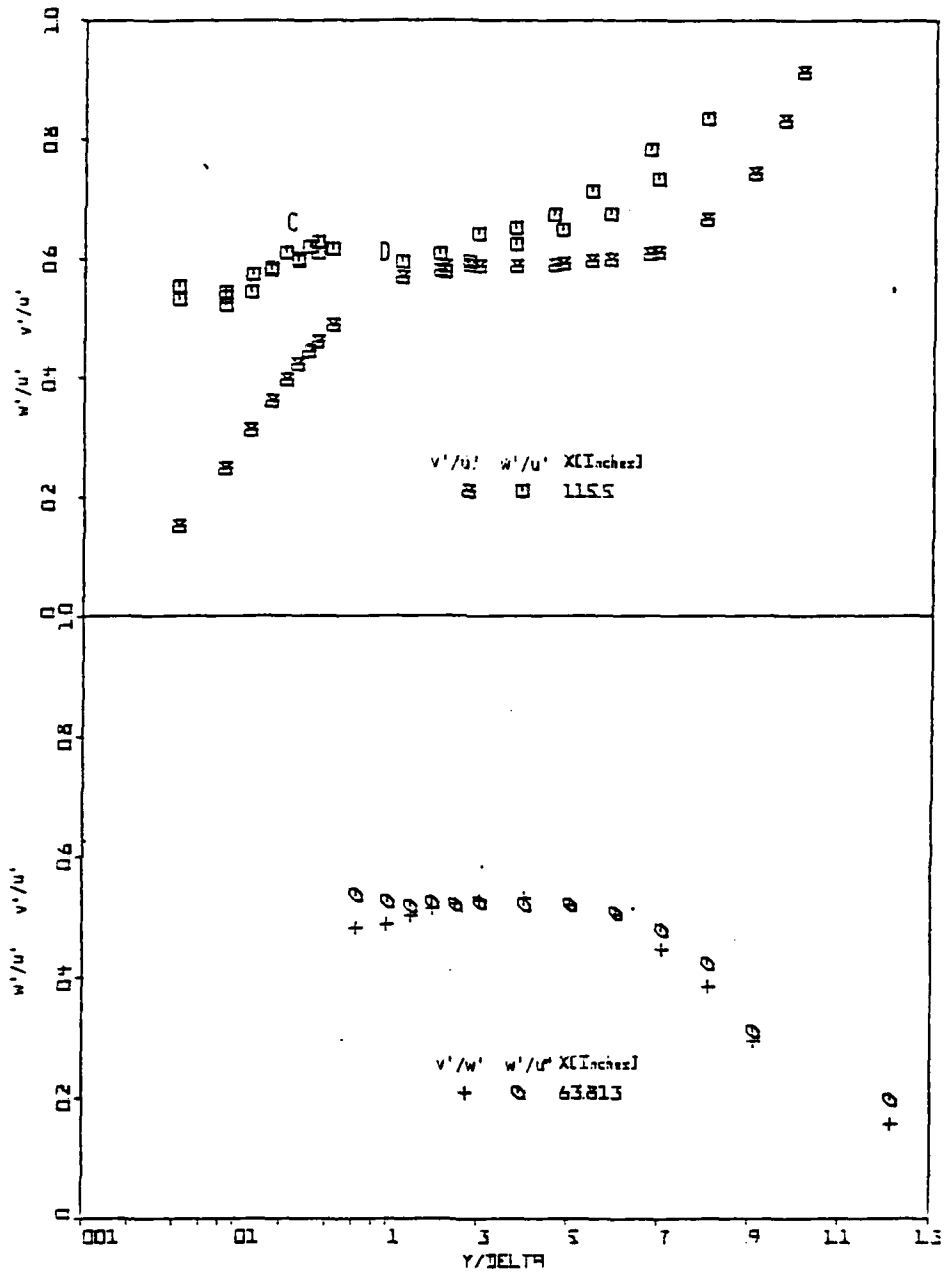


Figure 17(a). Distributions of v'/u' and w'/u' at the several streamwise locations. Note the log-linear abscissa.

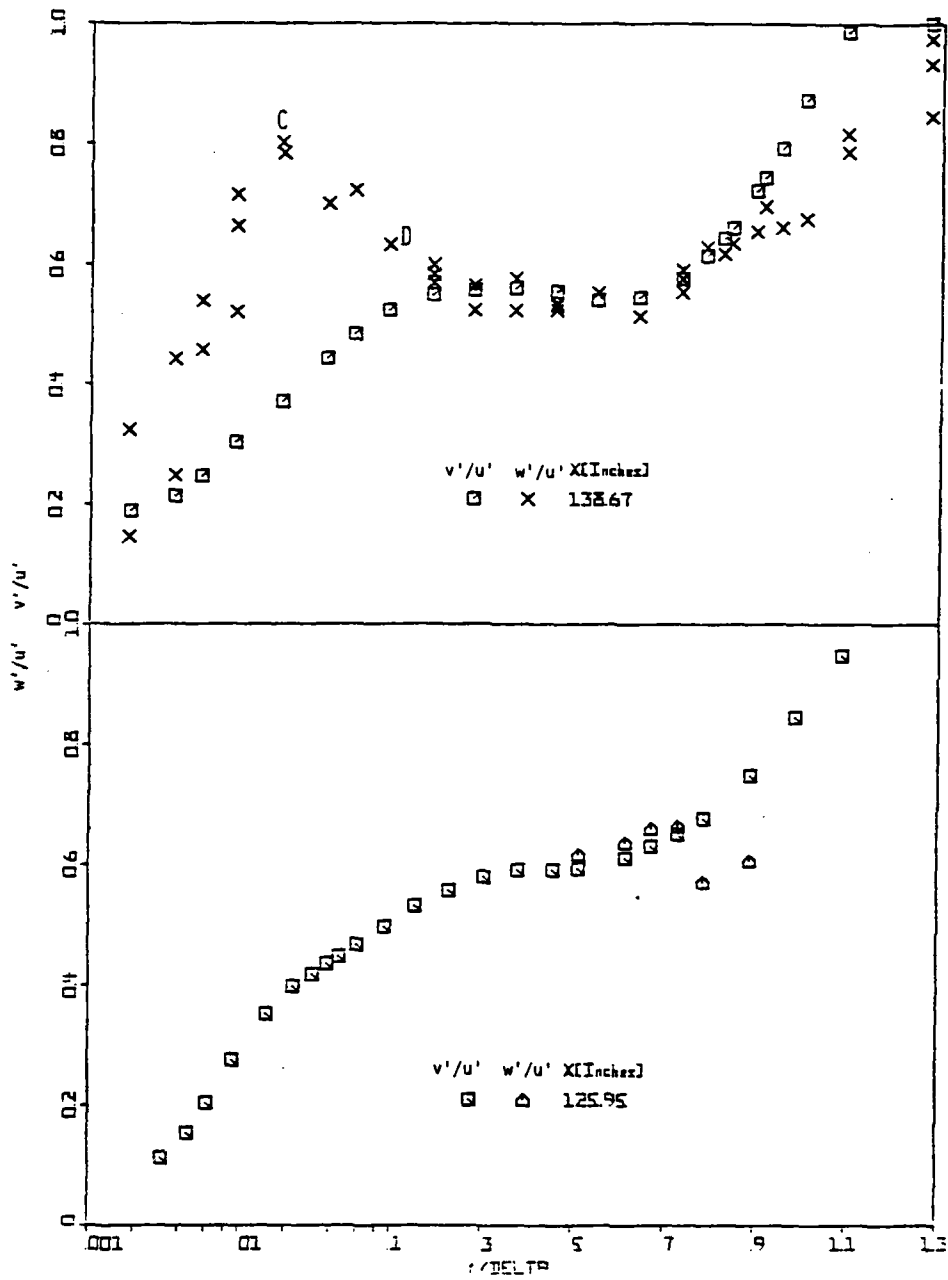


Figure 17(b). Distributions of v'/u' and w'/u' at the several streamwise locations. Note the log-linear abscissa.

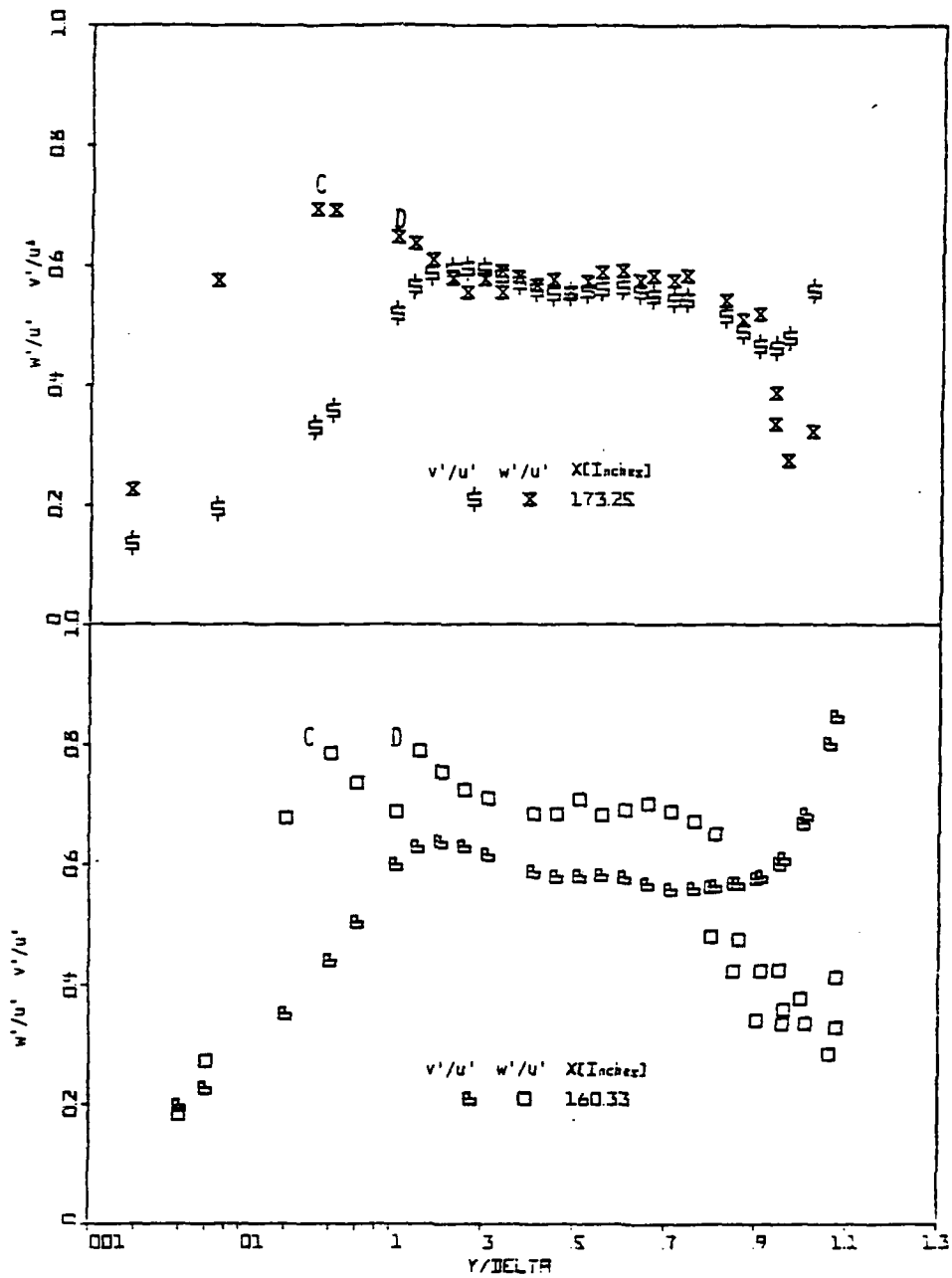


Figure 17(c). Distributions of v'/u' and w'/u' at the several streamwise locations. Note the log-linear abscissa.

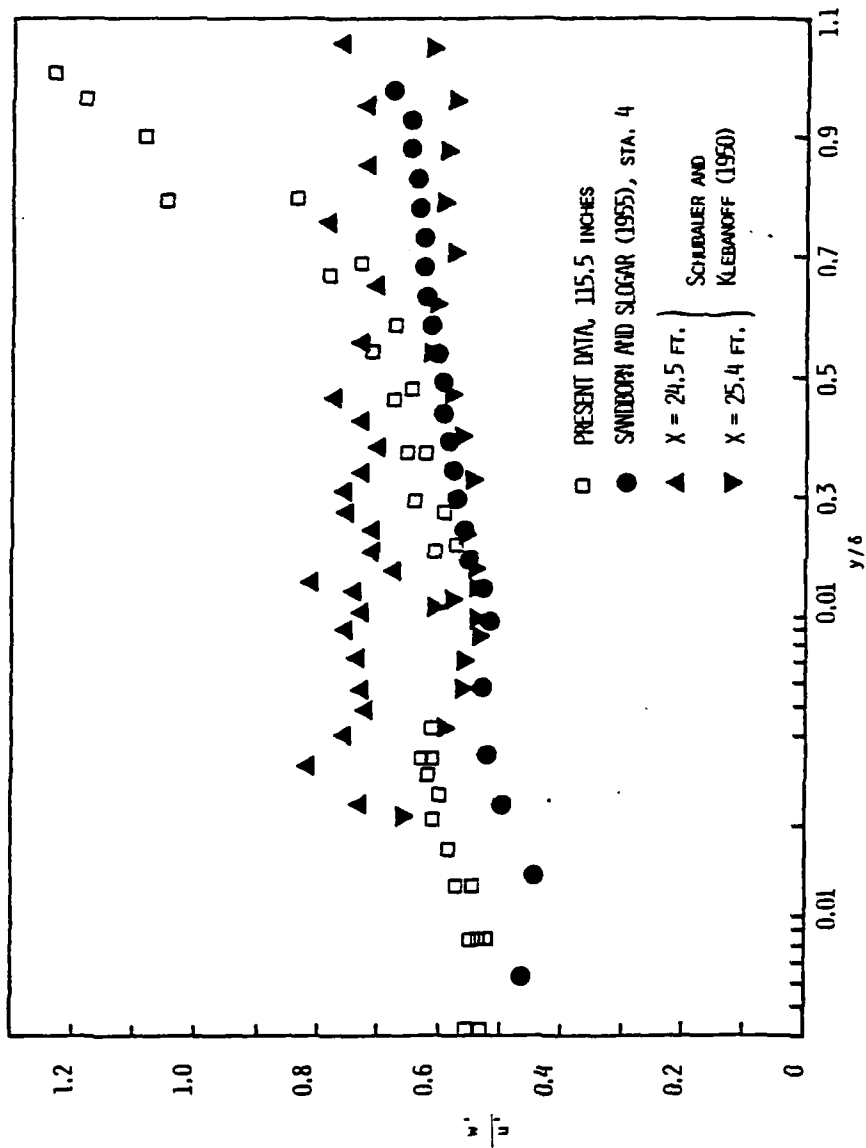


Figure 18. Comparison of present and previous w'/u' data upstream of separation for the conditions given in Table 3. Note the log-linear abscissa.

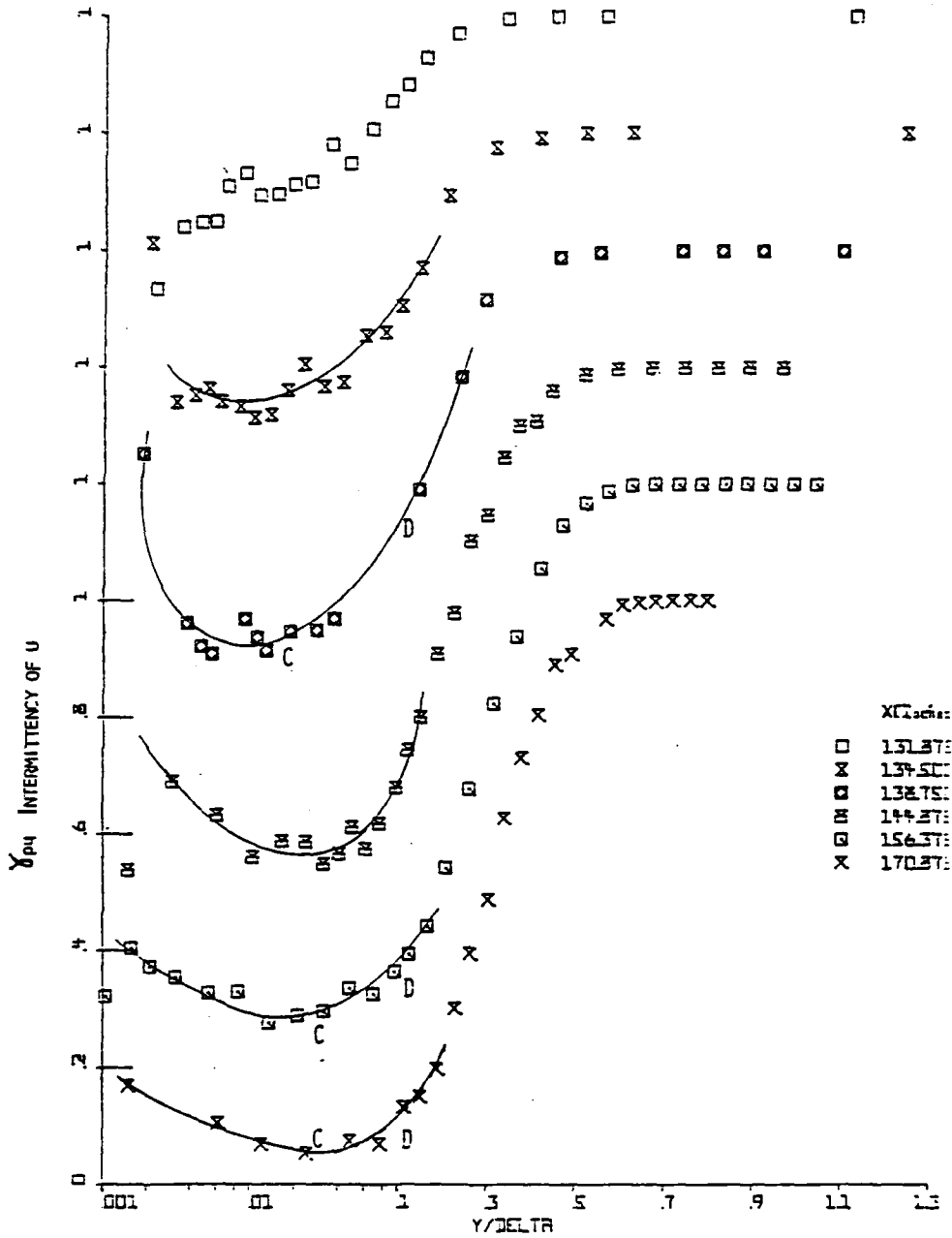


Figure 19. Streamwise intermittency γ_{pu} distributions with the locations of inflexion points C and D. Note the log-linear abscissa and the displaced ordinates.

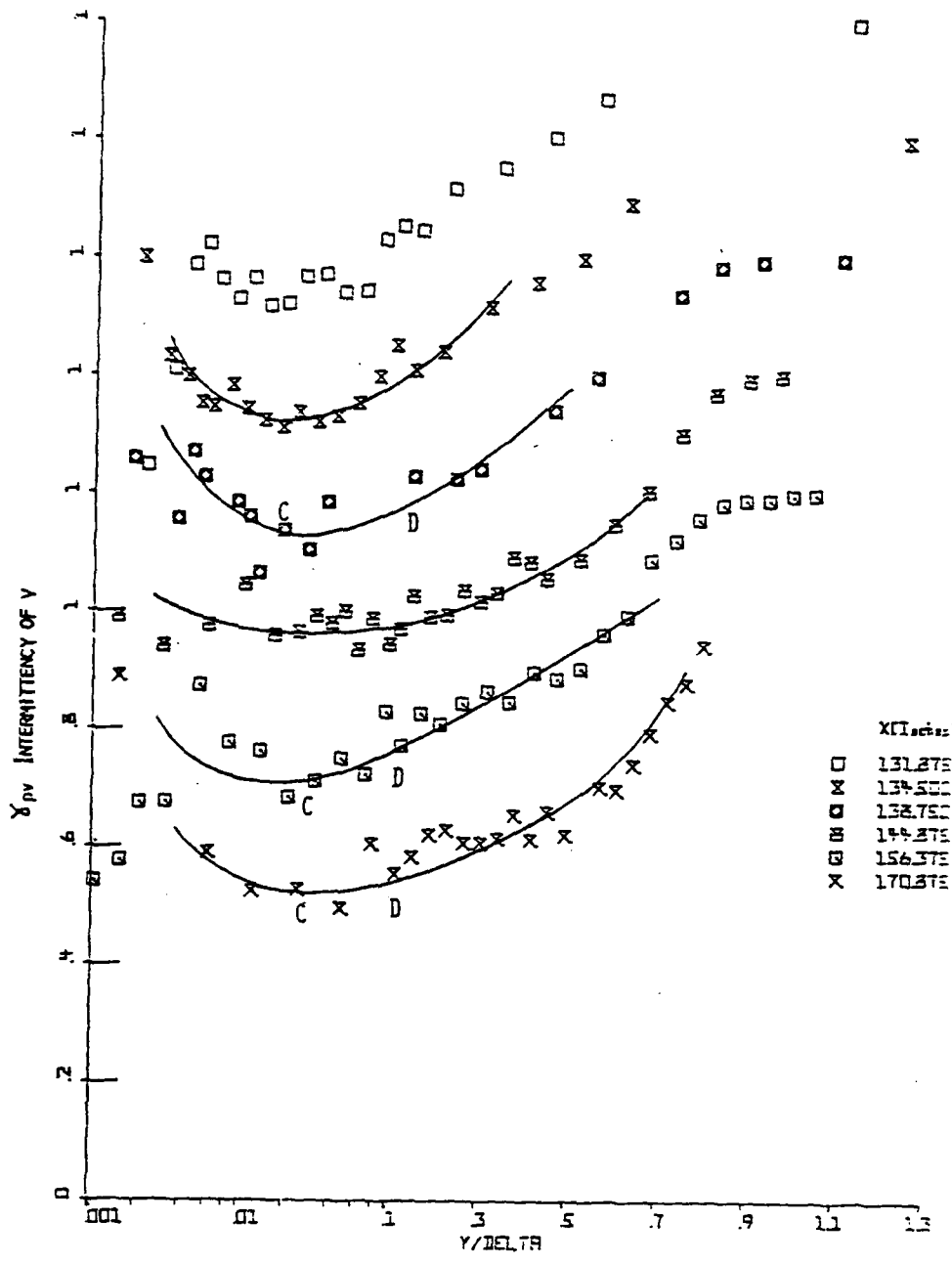


Figure 20. γ_{pv} distributions with the locations of inflexion points C and D. Note the log-linear abscissa and the displaced ordinates.

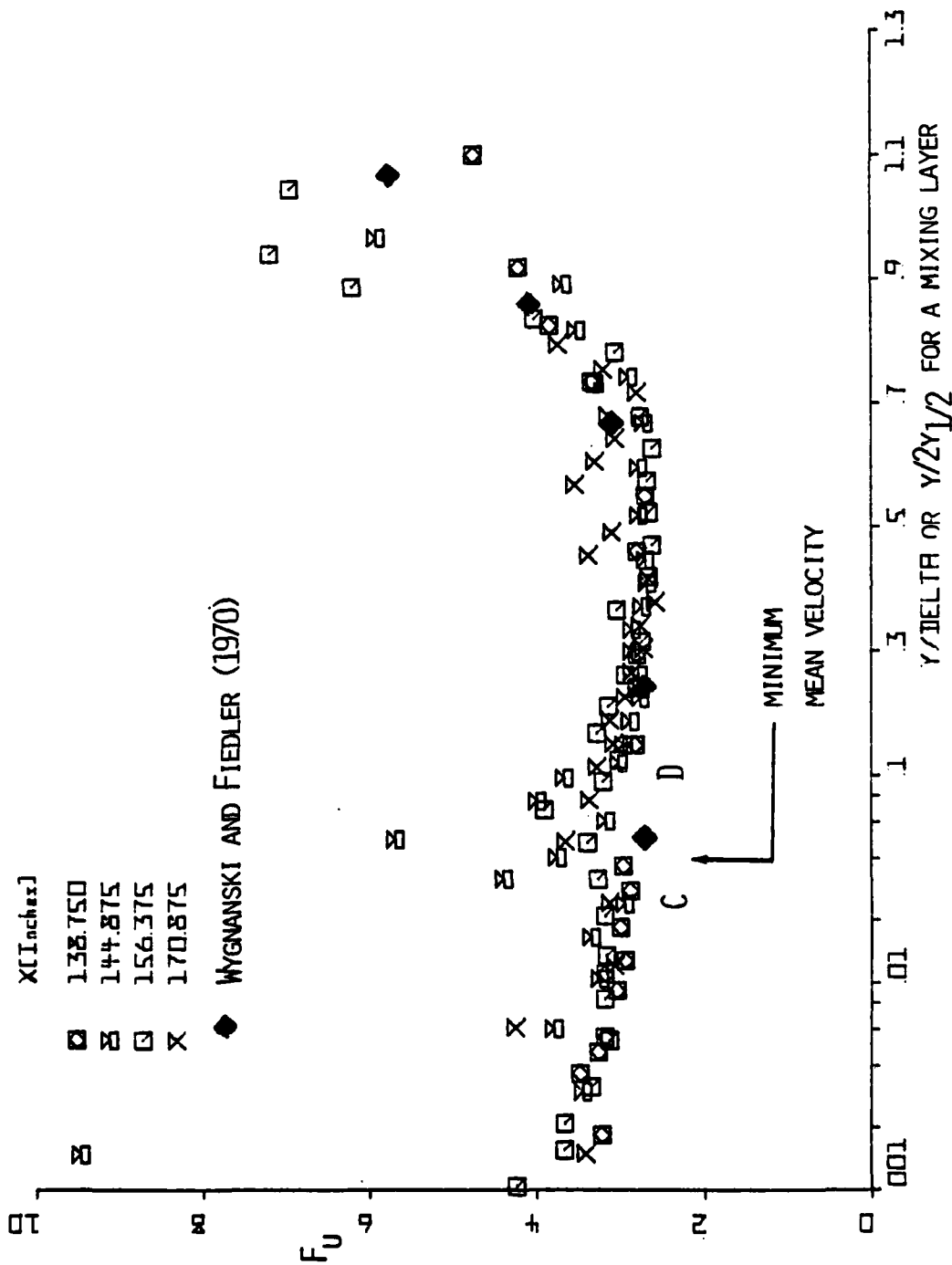


Figure 21. Flatness factor F_u profiles downstream of separation with the approximate locations of inflexion points C and D. Note the log-linear abscissa.

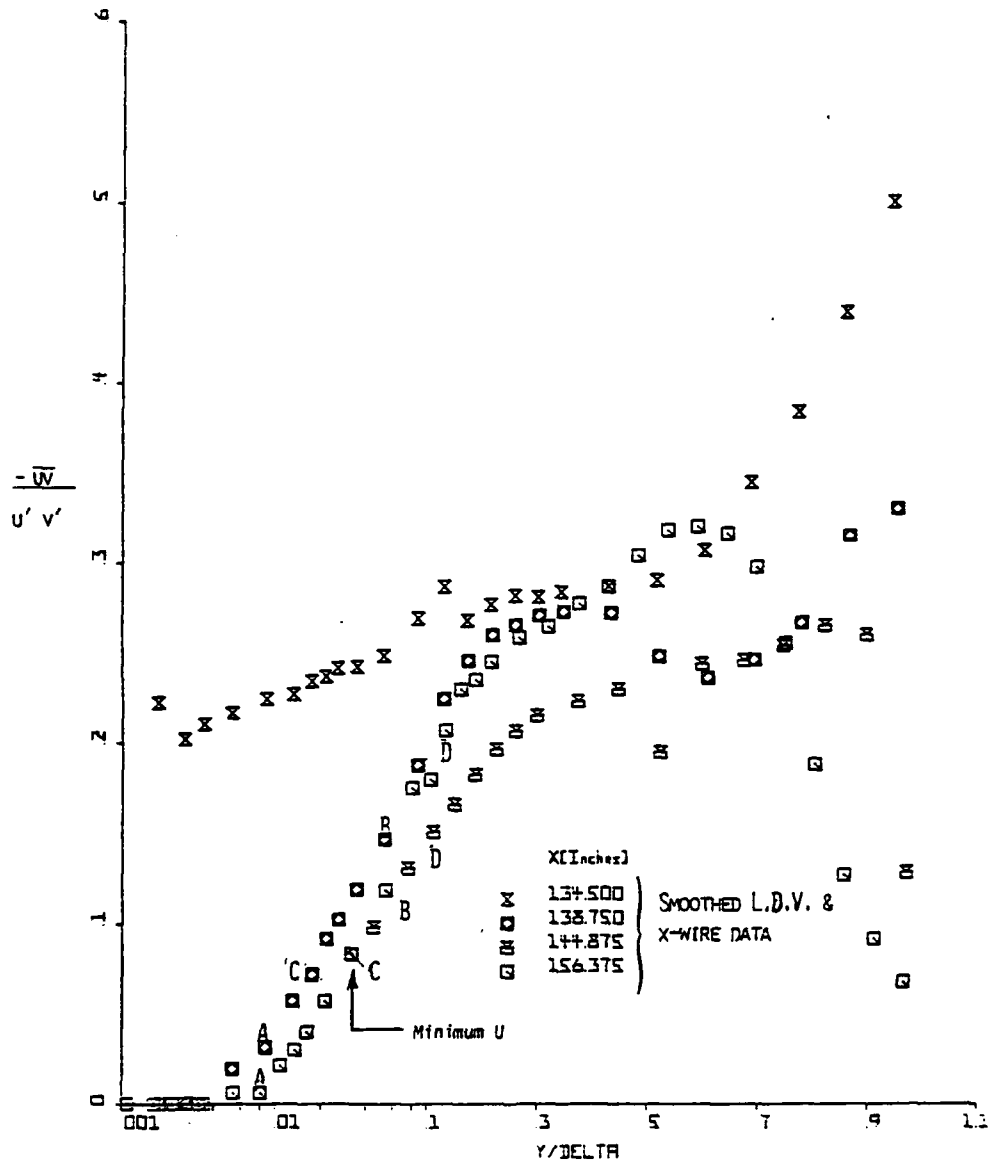


Figure 22. Reynolds shear stress correlation coefficient distributions with the locations of inflexion points. Note the log-linear abscissa.

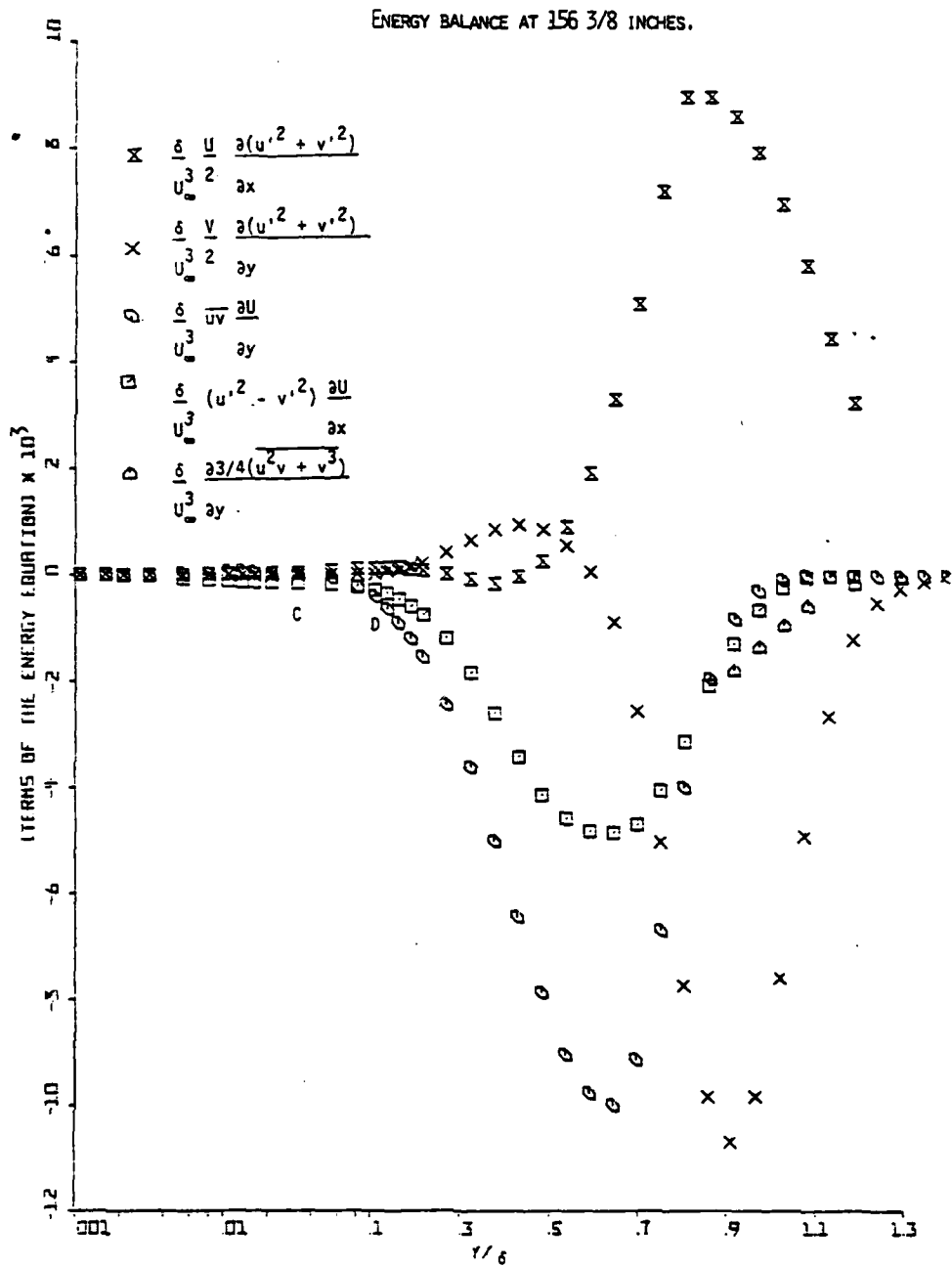


Figure 23. Turbulence energy balance downstream of separation with the locations of inflexion points C and D. Note the log-linear abscissa.

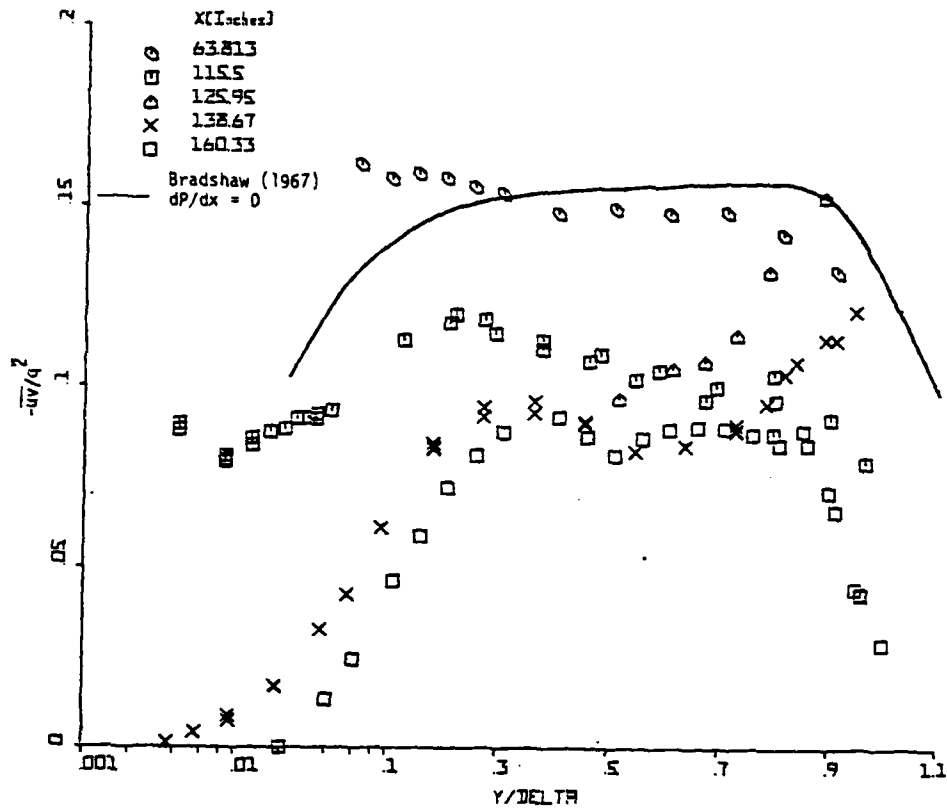


Figure 24. Turbulence energy correlation coefficient $-\overline{uv}/q^2$ distributions using the u'^2 , v'^2 and $-\overline{uv}$ data of Simpson et al. (1980) and the present w'^2 data.

UNCLASSIFIED

SECURITY CLASSIFICATION OF THIS PAGE (When Data Entered)

REPORT DOCUMENTATION PAGE		READ INSTRUCTIONS BEFORE COMPLETING FORM
1. REPORT NUMBER SMU-5-PU ✓	2. GOVT ACCESSION NO. AD-A095256	3. RECIPIENT'S CATALOG NUMBER
4. TITLE (and Subtitle) Measurements of the Transverse Velocity of a Separating Turbulent Boundary Layer		5. TYPE OF REPORT & PERIOD COVERED Technical March 1979-February 1980
		6. PERFORMING ORG. REPORT NUMBER
7. AUTHOR(s) Klara Shiloh, B.G. Shivaprasad, and R.L. Simpson		8. CONTRACT OR GRANT NUMBER(s) N00014-79-C-0277 ^{K5, D1}
9. PERFORMING ORGANIZATION NAME AND ADDRESS Southern Methodist University ✓ Dallas, Texas 75275		10. PROGRAM ELEMENT, PROJECT, TASK AREA & WORK UNIT NUMBERS
11. CONTROLLING OFFICE NAME AND ADDRESS Project SQUID Purdue University Chaffee Hall West Lafayette, Indiana 47907		12. REPORT DATE June 1980
		13. NUMBER OF PAGES 66
14. MONITORING AGENCY NAME & ADDRESS (if different from Controlling Office) Office of Naval Research-Power Program Code 473, Dept. of the Navy 800 No. Quincy Street Arlington, Virginia 22217		15. SECURITY CLASS. (of this report) Unclassified
		15a. DECLASSIFICATION/DOWNGRADING SCHEDULE
16. DISTRIBUTION STATEMENT (of this Report) This document has been approved for public release and sale; its distribution is unlimited.		
17. DISTRIBUTION STATEMENT (of the abstract entered in Block 20, if different from Report) Same		
18. SUPPLEMENTARY NOTES		
19. KEY WORDS (Continue on reverse side if necessary and identify by block number) Separation Turbulence Laser anemometer Fluid dynamics		
20. ABSTRACT (Continue on reverse side if necessary and identify by block number) (see reverse side)		

DD FORM 1 JAN 73 1473 EDITION OF 1 NOV 65 IS OBSOLETE

Unclassified

SECURITY CLASSIFICATION OF THIS PAGE (When Data Entered)

ABSTRACT

The problem of turbulent boundary layer separation due to an adverse pressure gradient is an old but still important problem in many fluid flow devices. Until recent years little quantitative experimental information was available on the flow structure downstream of separation because of the lack of proper instrumentation. The directionally-sensitive laser anemometer now provides the ability to accurately measure the instantaneous flow direction and magnitude.

Simpson, Chew, and Shivaprasad (1980) presented a number of experimental results for a nominally two-dimensional separating turbulent boundary layer for an airfoil-type flow in which the flow was accelerated and then decelerated until separation. Upstream of separation single and cross-wire hot-wire anemometer measurements were also presented. Measurements obtained in the separated zone with a directionally-sensitive laser anemometer system were

presented for U , V , $\overline{u^2}$, $\overline{v^2}$, $-\overline{uv}$, $\overline{u^3}$, $\overline{u^4}$, $\overline{v^3}$, $\overline{v^4}$, the fraction of time that the flow moves downstream, the fraction of time that the flow moves away from the wall, and u spectra. In addition to confirming the earlier conclusions of Simpson et al. (1977), these results provided new insights about the separated flow region.

From that work, the backflow appears to be supplied by the large eddy structure rather than coming from far downstream. It also was suggested that downstream of fully-developed separation the mean backflow could be divided into three layers: a viscous layer nearest the wall that is dominated by the turbulent flow unsteadiness but with little Reynolds shearing stress effects; a rather uniform mean velocity intermediate layer that seems to act as an overlap region between the viscous wall and outer regions; and the outer backflow region that is really part of the large-scaled outer region.

For the same flow this report presents experimental results for W , $\overline{w^2}$, $\overline{w^3}$, $\overline{w^4}$, and the fraction of time that the flow moves in one direction across the wind tunnel. A specially-designed directionally-sensitive laser anemometer that is described here was constructed and used to make measurements in the separated region. Cross-wire hot-wire anemometer measurements were obtained upstream of separation and in the outer region of the separated flow and are in good agreement with the laser anemometer results.

The results presented here support the earlier flow model of Simpson et al. (1980). Large scale structures that supply the mean backflow provide a plausible explanation of why u and w related quantities behave as they do in the three near-wall regions mentioned above. These large scale structures transport the turbulence energy to the backflow from the outer flow by turbulent diffusion. This is the main method of providing turbulence energy to the backflow since advection and production of turbulence kinetic energy is negligible there as compared to the dissipation rate.

